

1 **The impact of aerosols on photolysis frequencies and ozone**
2 **production in urban Beijing during the four-year period**
3 **2012–2015**

4 Wenjie Wang¹, Min Shao^{1,2*}, Min Hu¹, Limin Zeng¹, Yusheng Wu¹

5

6 1 State Joint Key Laboratory of Environmental Simulation and Pollution Control,
7 College of Environmental Sciences and Engineering, Peking University, Beijing
8 100871, China

9 2 Institute for Environmental and Climate Research, Jinan University, Guangzhou
10 511443, China

11

12

13

14

15

16

17 *** Correspondence to:**

18 Prof. Min SHAO

19 College of Environmental Sciences and Engineering, Peking University, Beijing
20 100871, China

21 Tel: +86-10-62757973; Fax: +86-10-62757973

22 Email: mshao@pku.edu.cn

23 **Abstract**

24 During the period 2012-2015, the photolysis frequencies were measured at the
25 Peking University site (PKUERS), a representative site of urban Beijing. We present a
26 study of the effects of aerosols on two key photolysis frequencies, $j(O^1D)$ and $j(NO_2)$.
27 Both $j(O^1D)$ and $j(NO_2)$ display significant dependence on AOD with a nonlinear
28 negative correlation. With the increase in AOD, the slopes of photolysis frequencies
29 vs AOD decrease, which indicates that the capacity of aerosols to reduce the actinic
30 flux decreases with AOD. In addition, the slopes are equal to $4.21-6.93 \cdot 10^{-6} s^{-1}$ and
31 $3.20 \cdot 10^{-3} s^{-1}$ per AOD unit for $j(O^1D)$ and $j(NO_2)$ respectively at SZA of 60° , both of
32 which are larger than those observed in the Mediterranean. This indicates that the
33 aerosols in urban Beijing have a stronger extinction on actinic flux than absorptive
34 dust aerosols in the Mediterranean. Since the photolysis frequencies strongly
35 depended on the AOD and the solar zenith angle (SZA), we established a parametric
36 equation to quantitatively evaluate the effect of aerosols on photolysis frequencies in
37 Beijing. According to the parametric equation, aerosols lead to a decrease in $j(NO_2)$
38 by 24.2% and 30.4% for summer and winter, respectively, and the corresponding
39 decrease in $j(O^1D)$ by 27.3% and 32.6% respectively, compared to an aerosol-free
40 atmosphere ($AOD = 0$). Based on an observation campaign in August 2012, we used
41 the photochemical box model to simulate the ozone production rate ($P(O_3)$). The
42 simulation results shows that the monthly average net ozone production rate is
43 reduced by up to 25% due to the light extinction of aerosols. Through further in-depth
44 analysis, it was found that particulate matter concentrations maintain high level under

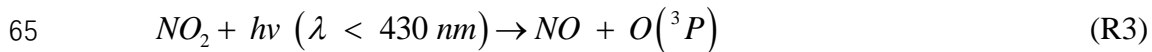
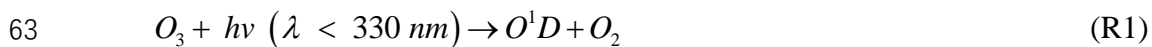
45 the condition of high concentrations of ozone precursors (VOCs and NO_x), which
46 inhibits the production of ozone to a large extent. This phenomenon implies a
47 negative feedback mechanism in the atmospheric environment of urban Beijing.

48

49

50 **1. Introduction**

51 Solar radiation plays an important role in atmospheric photochemistry, driving
52 the photolysis of many key species. The photolysis of ozone (O₃), gaseous nitrous
53 acid (HONO), and carbonyl species, which contributes to the primary production of
54 HO_x (Volkamer et al., 2010). The photolysis of ozone produces O¹D, which then
55 reacts with H₂O to form OH radicals; these radicals are the main source of OH
56 radicals in the troposphere, as shown by reactions R1 and R2. The strong dependence
57 of OH concentration on j(O¹D) was found in a number of field measurements (Ehhalt
58 et al., 2000; Rohrer et al., 2014; Stone et al., 2012). In addition, the photolysis of NO₂
59 produces O³P, and then O³P reacts with O₂ to produce O₃, as shown by reactions R3
60 and R4, which is the only significant source of ozone in the troposphere
61 (Finlayson-Pitts et al., 2000). The photolysis frequencies of R1 and R3 are j(O¹D) and
62 j(NO₂), respectively.





67 The photolysis frequencies are calculated by the following formula:

$$j = \int_{\lambda_1}^{\lambda_2} F(\lambda) \sigma(\lambda, S, T) \varphi(\lambda, S, T) d\lambda \quad (\text{E1})$$

69 $F(\lambda)$ is the actinic flux dependent on wavelength. Since the photolysis rates are
70 proportional to the actinic flux and not all stations acquire a 2π spectroradiometer or
71 chemical actinometers for J measurements, several methods have been developed to
72 determine actinic flux and photolysis frequencies from ground based measurements of
73 irradiance (Kylling et al 2003, Kazadzis et al. 2000, 2004, Topaloglou et al. 2005,
74 Trebs et al. 2009). $\sigma(\lambda, S, T)$ is the absorption cross section of the species that absorbs
75 in the wavelength range $\lambda_1-\lambda_2$. $\varphi(\lambda, S, T)$ is the quantum yield of the photodissociation
76 reaction product. λ , S and T represent wavelength, species and temperature,
77 respectively.

The effect of aerosols on photolysis frequencies depends on the aerosol optical properties, SZA and altitude (Liao et al., 1999). The aerosol optical depth (AOD) characterizes the integral of the extinction coefficient of aerosols in the vertical direction. The light extinction of aerosols includes scattering and absorption, which have different effects on the actinic flux. Scattering aerosols can enhance the actinic flux throughout the troposphere, while absorptive aerosols reduce the actinic flux throughout the boundary layer (Jacobson, 1998; Dickerson et al., 1997; Castro et al., 2001). To distinguish between these two components, single scattering albedo (SSA) is defined as the ratio of the scattering coefficient to the total extinction coefficient. In areas with severe aerosol pollution, aerosols can significantly affect photolysis

88 frequencies and ozone production. Studies in Los Angeles (Jacobson, 1998), Mexico
89 City (Castro et al., 2001; Raga et al., 2001; Li et al., 2011), São Paulo (de Miranda et
90 al., 2005), Huston (Flynn et al., 2010), Europe (Real et al., 2011) and Russia (Pere et
91 al., 2015) have found that aerosols reduce ozone concentration by 5-30% by
92 attenuating photolysis frequencies. Studies in the eastern United States have shown
93 that scattering aerosols increase ozone concentration by 5-60% by increasing the
94 photolysis frequencies (Dickerson et al., 1997; He and Carmichael, 1999). Therefore,
95 it is necessary to quantitatively evaluate the effect of aerosols on photolysis
96 frequencies for the purpose of effective ozone prevention.

97 Currently, the methods for quantitatively evaluating the influence of aerosols on
98 photolysis frequencies mainly include radiative transfer model and parameterization
99 method (Madronich et al., 1993). Radiative transfer model is based on an algorithm
100 for calculating solar radiation and photolysis frequencies (Madronich et al., 1999).
101 The observed data of related influential factors of the photolysis frequencies are taken
102 as the model's input and the photolysis frequencies simulated are compared with the
103 observed value to test the simulation effect. The method comprehensively considers
104 the influence of aerosol optical properties on the photolysis frequencies, but it does
105 not necessarily reflect the true quantitative relationship in the atmosphere due to
106 complicated environmental conditions and thus the simulated results don't necessarily
107 reproduce observed values well (Lefer et al., 2003; Shetter et al., 2003; Hofzumahaus
108 et al., 2004). For example, the simulated slope of $j(O^1D)$ vs AOD by Fast-JX
109 algorithm within the CHIMERE model was significantly smaller than the observed

110 slope, particularly for the high SZA values (Mailler et al., 2016). The parameterization
111 method is based on the observation data taken from a certain region and is used to
112 establish the parameterized relationship between the photolysis frequencies and
113 optical properties of aerosols (such as AOD). The method can reflect the actual
114 atmospheric environment conditions; it also considers less influential factors and thus
115 is easy to apply (Casasanta et al., 2011; Gerasopoulos et al., 2012). The disadvantage
116 of this method is that the established parametric equations apply only to a specific
117 region and cannot be extended to other regions.

118 With rapid economic development and urbanization in past decades, China's
119 atmospheric pollution has become more and more severe, characterized by high
120 concentrations of particulate matter and ozone. Satellite observations indicates that
121 both the particulate matter and the ozone of eastern China are at higher levels
122 compared with other locations in the globe (Verstraeten et al., 2015; Ma et al., 2014).
123 Levels of pollution in the Beijing–Tianjin–Hebei are even more severe (Chang et al.,
124 2009; Che et al., 2008; Zhang et al., 2014, Zhang et al., 2016). Therefore, it is
125 necessary to study the effects of aerosols on photolysis frequencies and ozone
126 production in the urban areas of China.

127 Previous model studies have shown that aerosols in China can affect ozone
128 production by changing the photolysis frequencies. Tang et al. (2004) used a sulfur
129 transmission–emission model (STEM) to discover that ozone concentration in
130 northeastern China was reduced by 0.1–0.8% in the sandstorm due to the change in
131 photolysis frequencies. Tie et al. (2005) used a global aerosol–chemical model to

132 show that aerosols caused $j(O^1D)$ and $j(NO_2)$ to decrease in winter by 20%-30% and
133 10%-30%, respectively, and in summer by 5%-20% and 1%-10%, respectively,
134 resulting in 2%-5% and 2% reductions in ozone concentration in winter and summer,
135 respectively. Li et al. (2011) used an air quality model to estimate the changes in the
136 photolysis rate caused by sulfate, nitrate, ammonium, and mineral dust aerosols in the
137 central and eastern regions of China from June 1 to June 12, 2006. This study showed
138 that the daily average $j(O^1D)$ in the troposphere at the altitude of 1 km, 3 km, and 10
139 km from the ground was reduced by 53.3%, 37.2%, and 20.9%, respectively, resulting
140 in a decrease in the ozone concentration by 5.4%, 3.8%, and 0.1% in the three layers.
141 Lou et al (2014) found that with aerosols, annual mean photolysis rates, $j(O^1D))$ and
142 $j(NO_2)$, were simulated to be reduced by 6-18% in polluted eastern China, leading to
143 reductions in O_3 of up to 0.5 ppbv in those regions in spring and summer by using the
144 global chemical transport model (GEOS-Chem). However, all of these studies base
145 their results on model simulations. Research using long-term observational data to
146 evaluate the effects of aerosols on photolysis frequencies and ozone production in
147 China has not yet been published.

148 Our overall goal is to quantitatively evaluate the effect of aerosols in urban
149 Beijing on photolysis frequencies and thus on ozone production. First, the relationship
150 between $PM_{2.5}$ and AOD was investigated. Second, based on long-term observations
151 (2012-2015) of photolysis frequencies, we discussed the impact of AOD on photolysis
152 frequencies ($j(O^1D)$ and $j(NO_2)$) in urban Beijing in detail. Then, the quantitative
153 relationship between photolysis frequencies, AOD, and SZA was acquired by the

154 parameterization method, which could be used to quantitatively evaluate the effect of
155 AOD on photolysis frequencies in Beijing. Finally, a photochemistry box model was
156 used to evaluate the effect of aerosols on ozone production.

157 **2. Methodology**

158 **2.1. Measurement**

159

160 From 2012 to 2015, $j(O^1D)$ and $j(NO_2)$ were measured continuously at PKUERS
161 site. The site ($39.99^\circ N$, $116.31^\circ E$) is located on the sixth floor of a campus building at
162 the Peking University, 20 km northwest of Tiananmen Square. The height from the
163 ground is about 30 m. The sampling point is surrounded by classroom buildings.
164 Concentration level and composition of air pollutants were thought to be similar to the
165 downtown so as to be representative for the whole of Beijing (Wang et al., 2010; Xu
166 et al., 2011; Zhang et al., 2012; Zhang et al., 2014).

167 The actinic flux was measured using a spectroradiometer and the photolysis
168 frequencies were calculated from the absorption cross section and quantum yield of
169 each species (Shetter and Muller, 1999). The spectroradiometer consisted of a single
170 monochromator with a fixed grating (CARL ZEISS), an entrance optic with a 2π
171 steradian (sr) solid angle quartz diffusor and a flexible optical quartz fiber bundle
172 connecting both components. The spectral measurements were performed with a
173 wavelength resolution of 2 nm, covering a wavelength range of 290-650 nm
174 (Hofzumahaus et al., 1999). The measured spectra were corrected for dark signal and

175 stray light. Descriptions of the calibration procedure and calculation of photolysis
176 frequencies are given in Bohn et al.(2008). The calculated photolysis frequencies had
177 a time resolution of 10 s and an uncertainty of $\pm 10\%$.

178 The optical properties of aerosols were measured by a CIMEL solar photometer
179 (AERONET level 2 data collection, <http://aeronet.gsfc.nasa.gov/>) and the site selected
180 was the Beijing-CAMS site (39.933°N , 116.317°E), which is close to the PKUERS
181 site. The CIMEL solar photometer is an automatic solar-sky scanning radiometer that
182 uses selected spectral channels. The instrumentation, data acquisition, retrieval
183 algorithms, and calibration procedure conform to the standards of the AERONET
184 global network and have been described in detail by Fotiadi et al. (2006). The solar
185 extinction measurement was performed every 3 minutes in the spectral range 340–
186 1020 nm for the calculation of AOD at wavelengths 340, 380, 440, 500, 675, 870, 970,
187 and 1020 nm. Under cloudless conditions, the overall uncertainty of AOD data is $\pm 1\%$
188 at $\lambda > 440$ nm and ± 0.02 at shorter wavelengths. In this study, AOD at the wavelength
189 of 380 nm was chosen for analysis. This wavelength was selected as it is more
190 representative of $j(\text{NO}_2)$. The SSA data were derived from a field campaign
191 undertaken in August 2012. The absorption and scattering coefficients were measured
192 with an Aethalometer (AE-31, Magee) and a Single Wavelength Integrating
193 Nephelometer (Aurora-1000), respectively, with a time resolution of 1 minute.
194 Five-minute averages of ozone column concentration, SSA, and photolysis
195 frequencies were analyzed in this study. The total ozone column was obtained by OMI
196 (Ozone Monitoring Instrument) for the year 2012-2015, using overpass data.

197 The analysis of the effects of aerosols on ozone production (Section 3.4) was
198 based on the field campaign undertaken in August 2012. The relevant contents and
199 methods of observation are shown in Table 1. In addition, meteorological parameters
200 such as temperature, humidity, and pressure were simultaneously observed at the site.
201 Since the time resolution of VOCs is 1 hour, all data analyzed in Section 3.4 was
202 processed as 1-hour average values. In this study, we focused on the effects of
203 aerosols on photolysis frequencies and ozone production under cloudless conditions.

204 **2.2 Radiative Transfer Model Description**

205 We use the Tropospheric Ultraviolet and Visible (TUV) radiation model
206 (version 5.3) provided by Sasha Madronich (Madronich, 1993). In order to solve the
207 radiative transfer equation, TUV uses the discrete-ordinates algorithm (DISORT) with
208 4 streams and calculates actinic flux spectra with wavelength range of 280-420 nm in
209 1 nm steps and resolution. Measured temperatures were used to calculate the
210 absorption cross sections and quantum yields. The key aerosol optical properties
211 including AOD, SSA and AE are input into the model to test the effect of aerosols on
212 photolysis frequencies. AE(380/550nm) is taken from AERONET and the mean value
213 of 1.3 during June 2012 - December 2015 is used in TUV model.

214

215 **2.3 Photochemical box model**

216 The photochemical box model used in this study is based on a regional
217 atmospheric chemical mechanism (RACM2) described by Goliff et al. (2013). The

218 mechanism includes 17 stable inorganic compounds, 4 intermediate inorganic
219 compounds, 55 stable organic compounds, and 43 intermediate organic compounds.
220 Compounds not specifically treated in RACM are incorporated into species with
221 similar functional groups. The isoprene-related mechanism used in this model is LIM
222 mechanism proposed by Peeters et al. (2009). In this study, the observed NO₂, CO,
223 SO₂, C₂–C₁₂ NMHCs, HCHO, photolysis frequencies, temperature, pressure, and
224 relative humidity were used as constraints to simulate the concentrations of reactive
225 radicals (RO₂, HO₂, and OH), intermediate species, and associated reaction rate
226 constants. HONO wasn't measured during the period and was calculated according to
227 the concentration of NO₂ and the observed ratio of HONO to NO₂ at an urban site in
228 Beijing, which had a marked diurnal cycle, a maximum in the early morning (ratio
229 values up to ~0.05–0.08 in summer) and a decrease during daytime to values around
230 0.01–0.02 (Hendrick et al., 2014). The model was spun up for two days once it started
231 running in order to ensure that the simulation was stable. It was assumed that the
232 lifetime of simulated species removed by dry deposit was 24 hours. The lifetime
233 corresponds to the assumed deposit rate of 1.2 cm s⁻¹ and a well-mixed boundary
234 layer height of about 1 km (Lu et al., 2012). Net ozone production is equal to the
235 reaction rate between peroxy radicals (RO₂ and HO₂) and NO minus the loss rate of
236 NO₂ and O₃ as shown in E2, E3, and E4. The ozone production rate (P(O₃)), the ozone
237 loss rate (D(O₃)), and the net P(O₃) were calculated from the simulation results.
238

$$239 \quad P(O_3) = k_{HO_2+NO} [HO_2] [NO] + \sum (k^i_{RO_2+NO} [RO_2^i] [NO]) \quad (E2)$$

240

$$D(O_3) = (\theta j(O^1 D) + k_{OH+O_3}[OH] + k_{HO_2+O_3}[HO_2] + \\ \Sigma(k^j_{alkene+O_3}[alkene^j]))[O_3] + k_{OH+NO_2}[OH][NO_2] \quad (E3)$$

242

$$net P(O_3) = P(O_3) - D(O_3) \quad (E4)$$

244

245 3. Results and discussion

246

247 3.1 The correlation between PM_{2.5} and AOD

248 In order to evaluate the extinction capacity of near-surface PM_{2.5}, we
 249 investigated the relationship between PM_{2.5} and AOD (at 380nm). The factors that
 250 affect this relationship include aerosol type, aerosol size distribution, aerosol
 251 distribution in the vertical direction, relative humidity (RH) and planetary boundary
 252 layer height (PBLH) (van Donkelaar et al., 2010). Figure 1 shows the correlation
 253 between AOD and PM_{2.5} in four different seasons. The determination coefficient (r^2)
 254 is 0.53, 0.58, 0.62 and 0.59 for spring (March, April and May), summer (June, July
 255 and August), autumn (September, October and November) and winter (December,
 256 January and February), respectively. Meanwhile, the correlation exhibits significant
 257 seasonal differences, having relatively smaller slope (23.56) in summer and relatively
 258 larger slope (73.76) in winter. This implies that the aerosols in summer have stronger
 259 extinction capacity than in winter. One reason for the seasonal differences is the

260 variation in RH among different seasons (Table 2). There is higher RH in summer
261 (57.2% on average) than in winter (30.4% on average), leading to stronger
262 hygroscopic growth of aerosol particles, and thus resulting in higher scattering ability
263 of aerosol particles. According to another study in urban Beijing, the higher the RH,
264 the smaller the slope, and the higher the PBLH, the smaller the slope (Zheng, C. W et
265 al., 2017). In addition, the slope was smaller for scattering-dominant aerosols than for
266 absorbing-dominant aerosols, and smaller for coarse mode aerosols than for fine mode
267 aerosols (Zheng, C. W et al., 2017). The slopes of the correlation between AOD (at
268 550nm) and PM_{2.5} in this study in summer and winter are equal to 42.2 $\mu\text{g m}^{-3}$ and
269 119.2 $\mu\text{g m}^{-3}$, respectively, close to that from Ma et al. (2016) (54.9 $\mu\text{g m}^{-3}$ and 110.5 μg
270 m^{-3}) and Xin et al. (2016) (55.2 $\mu\text{g m}^{-3}$ and 93.4 $\mu\text{g m}^{-3}$), but smaller significantly than
271 that from Zheng et al. (2017) (65~74 $\mu\text{g m}^{-3}$ and 143~158 $\mu\text{g m}^{-3}$). The differences
272 mainly depend on the aerosol composition and size distribution at different
273 observational sites in Beijing. Compared with other cities in North China (Tianjin,
274 Shijiazhuang and Baoding) (Ma et al., 2016), the slope in Beijing for winter is
275 significantly higher, indicating that the extinction capacity of aerosols in Beijing is
276 weaker in winter.

277

278

279 **3.2 Seasonal and diurnal variability of AOD and photolysis frequencies**

280 The diurnal cycles of AOD is shown in Figure 2. AOD displays obvious diurnal
281 variation, with relatively high level at noon and low level at dawn and evening. The

282 diurnal variation of PM_{2.5} is opposite to AOD. The opposite diurnal variation of AOD
283 and PM_{2.5} is mainly due to higher development of planetary boundary layer at noon,
284 resulting in more complete mixture of particulate matter in the vertical direction. In
285 addition, AOD has obvious seasonal differences, with the highest AOD in summer
286 and the lowest AOD in winter. Conversely, PM_{2.5} in winter ($66.9\mu\text{g m}^{-3}$) is
287 significantly higher than in summer ($45.5\mu\text{g m}^{-3}$). In spite of lower PM_{2.5} in summer,
288 AOD in summer is higher due to stronger extinction capacity of PM_{2.5} as discussed in
289 3.1. Figure 3 shows the diurnal variation of the photolysis frequencies under cloudless
290 conditions for each season. $j(\text{O}^1\text{D})$ and $j(\text{NO}_2)$ are both highest in summer, followed
291 by spring and autumn, and lowest in winter. This seasonal difference is mainly
292 determined by the difference in SZA for the four seasons.

293 The observed photolysis frequencies at this site are lower than that observed in
294 the eastern Mediterranean (Crete, Greece, $35^{\circ}20'\text{N}, 25^{\circ}40'\text{E}$) (Gerasopoulos et al.,
295 2012) by $7.8 \times 10^{-6}\text{ s}^{-1}$ and $4.9 \times 10^{-6}\text{ s}^{-1}$ for $j(\text{O}^1\text{D})$, and $1.9 \times 10^{-3}\text{ s}^{-1}$ and $3.3 \times 10^{-3}\text{ s}^{-1}$ for
296 $j(\text{NO}_2)$, in summer and winter respectively. The corresponding lower photolysis
297 frequencies of Beijing than the eastern Mediterranean due to SZA difference is $1.7 \times$
298 10^{-6} s^{-1} and $3.0 \times 10^{-6}\text{ s}^{-1}$ for $j(\text{O}^1\text{D})$, and $8.0 \times 10^{-5}\text{ s}^{-1}$ and $6.6 \times 10^{-4}\text{ s}^{-1}$ for $j(\text{NO}_2)$
299 according to TUV model, which are significantly lower than observed decreased
300 magnitudes. Taking into account the similar levels of ozone column concentration in
301 the two sites, the large gap of photolysis frequencies in the two sites is mainly
302 attributed to the higher AOD in Beijing (0.76 ± 0.75) than in the eastern Mediterranean
303 (0.27 ± 0.13).

304 It can be seen from Figure 3 that the difference between winter and summer for
305 $j(O^1D)$ is significantly larger than that for $j(NO_2)$, where the summer midday averages
306 of $j(O^1D)$ and $j(NO_2)$ are 5 times and 2 times those of winter, respectively. There are
307 two reasons for this phenomenon. One, compared with $j(NO_2)$, $j(O^1D)$ is more
308 sensitive to the change in SZA and the same change in SZA results in a larger change
309 in $j(O^1D)$ than $j(NO_2)$. Two, the main influential factors of $j(NO_2)$ under cloudless
310 conditions are SZA and AOD, and the influence of ozone column concentration and
311 temperature on $j(NO_2)$ is negligible. However, $j(O^1D)$ is affected significantly by the
312 ozone column concentration and temperature, in addition to SZA and AOD. The
313 higher ozone column concentration and lower temperature in winter than in summer
314 lead to the difference in $j(O^1D)$ further increasing (Table 2).

315

316

317 **3.3 The correlation between photolysis frequencies and AOD**

318 **3.3.1 The correlation between $j(O^1D)$ and AOD**

319 In order to rule out the effect of SZA on photolysis frequencies, we chose SZA
320 equal to 30° and 60° ($\pm 1^\circ$) for analysis. Figure 4 presents the dependence of $j(O^1D)$
321 on AOD at different levels of ozone column concentration at SZA of 30° and 60° (\pm
322 1°). The ozone column concentration has a classification width of 30 DU. This
323 relatively large classification width is chosen to make sure that there is enough points
324 to fit the relationship between $j(O^1D)$ and AOD. $j(O^1D)$ exhibits a clear dependence

325 on AOD, with a nonlinear negative correlation. The scatter of these points is mainly
326 due to variations in ozone column and temperature. As AOD increased, the slope of
327 $j(O^1D)$ -AOD gradually decreases, indicating that the ability of aerosols to reduce
328 $j(O^1D)$ gradually decreases with AOD. This result differs from that found in
329 Mediterranean, where $j(O^1D)$ was linearly negatively correlated with AOD (Casasanta
330 et al., 2011; Gerasopoulos., 2012). A larger variation range of AOD in Beijing (0-3)
331 compared with Mediterranean (0-0.6) is one reason for the difference.

332 For further analysis, the observed relation between $j(O^1D)$ and AOD was
333 compared with TUV-simulated results. Panels a and b of Figure 5 present the
334 comparison between observed and TUV-simulated $j(O^1D)$ against AOD at a SZA of
335 30° and 60° respectively and ozone column concentration of 330-360 DU. At low
336 AOD level (< 0.8), the observed slope of $j(O^1D)$ vs AOD is significantly larger than
337 the simulated slope at SSA of 0.95, and slightly larger than the simulated slope at SSA
338 of 0.85. With AOD increasing, the observed slope decreases rapidly to the level
339 smaller than the simulated slopes. The rapid change of the slope with AOD can be
340 related to the variation of SSA at different AOD level. Figure 6 presents the
341 relationship between SSA and AOD based on observed data in August 2012. The
342 result suggests a significant correlation between SSA and AOD. With the increase in
343 AOD, SSA is elevated; meanwhile, the slope of SSA vs AOD is gradually reduced.

344 Similar results have been obtained by Bais et al., 2005, Krotkov et al., 2005 and
345 Kazadzis et al., 2012. SSA characterizes the ratio of the scattering extinction
346 coefficient to the total extinction coefficient (scattering extinction coefficient plus

absorptive extinction coefficient) of aerosols. The smaller the SSA, the higher the absorptive component and lower the scattering component of the aerosol, and the stronger the ability of the aerosol to reduce the actinic flux (Dickerson et al., 1997).
Figure 6 indicates that aerosols in Beijing under low AOD conditions had a higher proportion of absorptive aerosol components than under high AOD conditions, and, as a result, had a stronger ability to reduce the photolysis frequencies, which contributed to the rapidly reduced slope of $j(O^1D)$ vs AOD with AOD. However, due to absence of more SSA data of the period 2012-2015, we can't give more sufficient evidence for the dependence of SSA on AOD. For another perspective, Owing to the biomass burning and soot emission generated from heating, the fine mode heavily-absorbing aerosol percentage is higher in winter than in summer (Zheng et al., 2017; Liu et al., 2016; Zhang et al., 2013), and thus aerosols in winter have stronger ability to reduce the photolysis frequencies. High AOD levels often appeared in summer and low AOD levels occurred mostly in winter (Figure 2), another fact that may also explains the rapidly reduced slope of $j(O^1D)$ vs AOD with AOD.

Comparing panels a and b of Figure 4, we see that at AOD smaller than 1, the slope of $j(O^1D)$ vs AOD exhibits a significant dependence on SZA and the slope at 30° of SZA is about 1.5-2.0 times larger than that at 60° of SZA. This result is similar to that of the observations made in the central Mediterranean (Casasanta et al., 2011). For the purpose of comparison with the study in the Mediterranean, the slope of $j(O^1D)$ vs AOD was calculated at AOD smaller than 0.7.

368 Table 3 presents slope, intercept and the determination coefficient (r^2) of linear
369 fits of correlation between $j(O^1D)$ and AOD for each ozone column class at AOD
370 smaller than 0.7. At SZA of 60° and O₃ column concentration of 300-330 DU, the
371 respective slope of the linear regression indicates a reduction of $j(O^1D)$ by $4.21 \cdot 10^{-6}$
372 s⁻¹ per AOD unit. Gerasopoulos et al. (2012) reported that the observed slope in the
373 eastern Mediterranean was equal to $2.44 \cdot 10^{-6}$ s⁻¹ at O₃ column of 300-320 DU.
374 Casasanta et al. (2011) reported that the observed slope in the central Mediterranean
375 varied from $2.66 \cdot 10^{-6}$ s⁻¹ to $3.87 \cdot 10^{-6}$ at O₃ column of 300-330 DU. All of these results
376 are smaller than the value of the present study, indicating that aerosols in urban
377 Beijing had a stronger extinction capacity on $j(O^1D)$ than those in the Mediterranean
378 that was influenced by both natural absorptive aerosols and anthropogenic aerosols.
379 Previous study indicated that SSA in Beijing ranged from 0.80 to 0.86 (Garland et al.,
380 2009; Han et al., 2015b; Han et al., 2017; Tian et al., 2015). The relatively low SSA in
381 Beijing could be an important reason for the stronger extinction capacity.

382

383

384 **3.3.2 The correlation between $j(NO_2)$ and AOD**

385 Unlike $j(O^1D)$, $j(NO_2)$ is negligibly affected by ozone column concentration and
386 depends mainly on AOD and SZA under cloudless conditions. Figure 7 presents the
387 dependence of $j(NO_2)$ on AOD at different SZA levels under cloudless conditions.
388 The cosine of SZA ($\cos(SZA)$) is categorized according to a width of 0.2. In the same

389 category of cos (SZA), $j(\text{NO}_2)$ displays a strong dependence on AOD. The scatter of
390 these points is due to the relatively large classification width of SZA to a large extent.
391 When $\cos(\text{SZA})$ is at its maximum level (0.8–1), the correlation between $j(\text{NO}_2)$ and
392 AOD is close to linear. When $\cos(\text{SZA})$ decreases, the correlation tends to be
393 nonlinear. Similar to $j(\text{O}^1\text{D})$, the observed slopes of $j(\text{NO}_2)$ vs AOD are also larger
394 than TUV-simulated slope at SSA of 0.95 and 0.85 when AOD is smaller than 0.8,
395 and decreased rapidly with increasing AOD (panels c and d of Figure 5). The reason
396 for this result is the same with that for $j(\text{O}^1\text{D})$ as explained above.

397 Table 4 presents the slope, intercept and the determination coefficient (r^2) of
398 linear fits of correlation between $j(\text{NO}_2)$ and AOD for each ozone column class at
399 AOD smaller than 0.7. The slope of $j(\text{NO}_2)$ vs AOD also displays a significant
400 dependence on $\cos(\text{SZA})$. The slope increases as $\cos(\text{SZA})$ increases from 0 to 0.5
401 and then decreases as $\cos(\text{SZA})$ increases from 0.5 to 1. At SZA of $60^\circ \pm 1$ (\cos
402 ($\text{SZA})=0.5 \pm 0.015$), the respective slope of the linear regression indicates a reduction
403 of $j(\text{NO}_2)$ by $3.2 \cdot 10^{-3} \text{ s}^{-1}$ per AOD unit. This result is larger than the value for non-dust
404 aerosols ($2.2 \cdot 10^{-3} \text{ s}^{-1}$) and close to the value for dust aerosols ($3.1 \cdot 10^{-3} \text{ s}^{-1}$) in the
405 eastern Mediterranean reported by Gerasopoulos et al. (2012).

406

407 **3.4 The parameterization relationship between photolysis frequencies, AOD, and**
408 **SZA**

409

410 As analyzed above, the photolysis frequencies ($j(O^1D)$ and $j(NO_2)$) strongly
411 depended on AOD and $\cos(SZA)$ and could be fit into expression E5 using a quadratic
412 polynomial form. Table 5 and Table 6 presents the fitting parametric equations and the
413 corresponding coefficients of determination (R^2) at different O_3 column ranges. The
414 coefficients of determination of the fitting equations are greater than 0.95 for $j(NO_2)$
415 and $j(O^1D)$, indicating that both of the photolysis frequencies strongly depended on
416 AOD and $\cos(SZA)$ at a certain O_3 column, and the effect of other factors such as
417 SSA and AE are integrated into the constant term in the parametric equation. Since the
418 ozone column concentration has greater influence on $j(O^1D)$ than on $j(NO_2)$, the
419 parameters of fitting equations for $j(NO_2)$ are similar, but the parameters of fitting
420 equations for $j(O^1D)$ have a large fluctuation at different O_3 column ranges (especially
421 a_1 and a_2). The parametric equations can be used to quantitatively evaluate the effect
422 of AOD on photolysis frequencies in Beijing. According to the parametric equations,
423 aerosols lead to a decrease in $j(NO_2)$ by 24.2% and 30.4% and a decrease in $j(O^1D)$ by
424 27.3% and 32.6% in summer and winter, respectively, compared to an aerosol-free
425 atmosphere. The decreasing ratio of the photolysis frequencies in winter is higher than
426 in summer due to the higher SZA and lower SSA in winter.

427 The effect of aerosols on photolysis frequencies in Beijing is compared with
428 other studies. Real and Sartelet (2011) reported a reduction in $j(NO_2)$ and $j(O^1D)$ of
429 13%-14% due to aerosols by using the radiative transfer code Fast-J during summer
430 2001 over European regions. Flynn et al (2010) reported that aerosols reduced $j(NO_2)$
431 by 3% in Huston during 2006 by using TUV model. Gerasopoulos et al (2012)

432 reported that aerosols reduced $j(\text{NO}_2)$ and $j(\text{O}^1\text{D})$ by 5%-15% with 5-yr mean AOD at
433 380nm equal to 0.27. All of these results are lower than the reduction ratio of this
434 study mainly due to higher aerosol level in Beijing (4-yr mean AOD equal to $0.76 \pm$
435 0.75). Hodzic et al. (2007) simulated a 15–30% $j(\text{NO}_2)$ photolysis reduction during
436 the 2003 European summer heatwave in the case of absorbing biomass burning
437 aerosols with AOD at 550 nm equal to 0.7-0.8 and SSA at 532 nm equal to 0.83-0.87.
438 The result of Hodzic et al. (2007) is comparable with the reduction ratio of this study
439 possibly due to the equivalent levels of AOD and SSA. In addition, Péré et al (2015)
440 simulated a higher reduction (20–50%) in $j(\text{NO}_2)$ and $j(\text{O}^1\text{D})$ along the transport of
441 the aerosol plume during the 2010 Russian summer wildfires episode. The higher
442 reduction is due to the higher level of AOD (peak value of AOD at 400nm reached
443 2-4), even though SSA is very high (0.97).

444
$$j = a_1 + a_2 \text{AOD} + a_3 \cos(SZA) + a_4 (\text{AOD})^2 + a_5 \text{AOD} \cos(SZA) + a_6 (\cos(SZA))^2 \dots \text{E5}$$

445

446 The above established parametric relationship of $\text{PM}_{2.5}$ -AOD and
447 $j(\text{NO}_2)$ -AOD-SZA gives us a chance to estimate the effect of $\text{PM}_{2.5}$ on photolysis
448 frequencies due to aerosol light extinction.

449 **3.5 The influence of AOD on ozone production**

450

451 In order to explain the effect of aerosol light extinction on ozone production, we
452 used the data from the field observation campaign undertaken in August 2012. Ozone

453 production depends on its precursors (NO_x and VOCs), meteorological factors, and
454 solar radiation. Solar radiation is the driving force for tropospheric photochemical
455 reactions, in which $j(O^1D)$ and $j(NO_2)$ are both important for ozone production. On
456 the one hand, the increase in $j(NO_2)$ promotes the photolysis of NO₂, thereby
457 accelerating the formation of ozone. On the other hand, the increase in $j(O^1D)$
458 accelerates the photolysis of ozone. In addition, the increase in the photolysis
459 frequencies will accelerate the photolysis of OVOC (especially formaldehyde and
460 acetaldehyde), HONO, and H₂O₂, resulting in increases in OH and HO₂, which will
461 promote the reaction between OH and VOCs and thus produce more RO₂. As a result,
462 more ozone is produced by increasing the reaction rate between RO₂ (or HO₂) and NO.
463 However, the increase in OH and HO₂ also consumes ozone and NO₂, which
464 contributes to the increase in D(O₃). In brief, the overall effect of changes in
465 photolysis frequencies on sources and sinks of ozone determines the change in the net
466 ozone production rate.

467 Ozone production (HO₂ + NO, RO₂ + NO), ozone loss (O¹D + H₂O, HO₂ + O₃,
468 O₃ + OH, NO₂ + OH, and O₃ + alkenes), and net ozone production rate during August
469 2012 were calculated by using the box model. We used the observed photolysis
470 frequencies (i.e. j_{obs}) and the calculated photolysis frequencies by parametric
471 equation under the condition of AOD equal to 0 (i.e. $j_{AOD=0}$), were used to
472 constrain the box model. The difference of simulated results in the two scenarios can
473 be attributed to the effect of aerosol light extinction. As a result, the presence of
474 aerosols causes a decrease in both ozone production rate and loss rate, as is shown in

475 Figure 8. Since the decreasing amplitude of the ozone production rate is far larger
476 than that of the ozone loss rate, the net production rate of ozone is reduced by 25%.
477 This reduction is comparable with the results of the study in Mexico City, where
478 aerosols caused a 20% reduction in the ozone concentrations (Castro et al., 2001).
479 Studies in Houston and Crete have shown that aerosols cause ozone production rates
480 to decrease by about 4% and 12%, respectively, which are lower than that found in
481 this study (Flynn et al., 2010; Gerasopoulos et al., 2012).

482 The ratio of the observed photolysis frequencies to the photolysis frequencies at
483 AOD equal to 0 is defined as JIF (Flynn et al., 2010). A JIF of less than 1 indicates
484 that the aerosols cause a decrease in the photolysis frequencies. Figure 9 shows the
485 relation between $P(O_3)_{j_obs}/P(O_3)_{j_AOD=0}$ (or $D(O_3)_{j_obs}/D(O_3)_{j_AOD=0}$) and JIF. The
486 majority of JIF values were less than 1, with an average of 0.72, indicating that
487 aerosols greatly attenuated photolysis frequencies due to high levels of AOD (average
488 of 1.07) and low levels of SSA (average of 0.84) during the observation period.
489 $P(O_3)_{j_obs}/P(O_3)_{j_AOD=0}$ and $D(O_3)_{j_obs}/D(O_3)_{j_AOD=0}$ are both linearly positively
490 correlated with JIF and the scatters are mostly above the 1:1 line. As can be seen from
491 the figure 9, a 30% reduction in photolysis frequencies (JIF = 0.7) due to the presence
492 of aerosols results in a decrease in ozone production rate and loss rate by about 26%
493 and 15%, respectively. The decreasing amplitude in the ozone production rate is
494 greater than the decrease in the ozone loss rate because the corresponding processes
495 of ozone production are all light-driven, but the corresponding processes of ozone loss
496 are not all light-driven because the reaction of O_3 with alkenes does not depend on

497 solar radiation. According to the simulated results, the reaction of ozone with alkenes
498 during this campaign accounts for 17% of total ozone loss.

499 The diurnal profile of the mean ozone production and loss rate is shown in
500 Figure 10. $P(O_3)$ peak midday in the 12:00-14:00 local hours at 31 ppb/h without
501 aerosol impact and 23 ppb/h with aerosol impact. The maximum $D(O_3)$ also occurs
502 between 12:00 and 14:00 at 4.2 ppb/h without aerosol impact and 3.5 ppb/h with
503 aerosol impact. There is little difference between aerosol-impact and aerosol-free
504 $P(O_3)$ (or $D(O_3)$) in the hours of 6:00-11:00, but the difference in the afternoon
505 (12:00-18:00) is large, indicating that the reduction effect of aerosol on ozone
506 production mainly occurs during the afternoon.

507 The above analysis focuses on the effect of aerosol on the ozone production due
508 to aerosol light extinction. However, it does not consider the close relationship
509 between aerosol and ozone's gaseous precursors in the actual atmosphere. To explain
510 this problem, we chose two adjacent days (small SZA effect) with obviously different
511 AOD levels: a clean day (A day: August 21, 2012; AOD = 0.21, $PM_{2.5}=21.6 \mu g m^{-3}$)
512 and a day with high aerosol pollution (B day; August 26, 2012; AOD = 3.2,
513 $PM_{2.5}=125.0 \mu g m^{-3}$) (Table 7). The difference in AOD between the two days can be
514 taken to represent the maximum daytime gap of AOD for this month. The ozone
515 column concentrations for these two days were 302 DU and 301 DU, respectively, of
516 which the effect on $j(O^1D)$ is negligible. Under these conditions, the $j(O^1D)$ value at
517 noon time decreases from $3.23 \times 10^5 s^{-1}$ on A day to $1.29 \times 10^5 s^{-1}$ on B day (i.e., a 60%
518 reduction) and the $j(NO_2)$ value at noon time decreases from $8.26 \times 10^{-3} s^{-1}$ on A day

519 to $4.19 \times 10^{-3}\text{s}^{-1}$ on B day (i.e., a 49.2% reduction). As shown in Table 7, B day has
520 higher AOD and higher concentrations of gaseous pollutants. The concentrations of
521 CO, NO₂, HCHO and the OH reactivity of VOCs in B day are much higher than in A
522 day, with the ratio of 3.6, 2.3, and 2.0, respectively. The simultaneous increases of
523 gaseous pollutants and AOD are due to the fact that gaseous pollutants (NO_x, SO₂,
524 and VOCs) emitted by major pollution sources in Beijing, including traffic and
525 industry, have undergone the processes of gas-phase oxidation and nucleation to
526 generate secondary particulate matter that contributes to aerosol light extinction.
527 Previous studies have reported that secondary particulate matter has accounted for
528 more than 60% of total particulate matter during severe smog pollution in Beijing
529 summers (Han et al., 2015a; Guo et al., 2014). In addition, several studies have shown
530 that secondary components in particulate matter (especially secondary organics and
531 ammonium sulfate) have dominated the aerosol light extinction (Han et al., 2014; Han
532 et al., 2017; Wang et al., 2015). Observations made in Beijing during the summer of
533 2006 showed that ammonium sulfate and ammonium nitrate contributed 44.6% and
534 22.3%, respectively, to the total extinction coefficient during a severe period of smog
535 (Han et al., 2014); in the summer of 2014 in Beijing, ammonium sulfate, secondary
536 organic aerosols, and ammonium nitrate contributed 30%, 22%, and 18%, respectively,
537 to the total extinction coefficient (Han et al., 2017).

538 As shown in Figure 11, the simulation results indicate that the net P(O₃) of B day
539 is 36.2% higher than that of A day due to higher concentrations of ozone precursors
540 on B day. This result is consistent with the observed ozone concentrations, of which

541 the observed ozone concentration in B day is 2.2 times higher than that of A day. If we
542 adjust the photolysis frequencies level of B day to the level of A day, the net P(O₃)
543 increases by 70.0%, which indicates that the high level of particulate matter in B day
544 greatly inhibits ozone production. This result means that the system is under negative
545 feedback, thus keeping O₃ at a relatively stable level. Table 8 summarizes the average
546 levels of gaseous pollutants and photolysis frequencies for AOD less than 1 and
547 greater than 1, as measured during August 2012. It shows that, the concentrations of
548 ozone's precursors are higher and the photolysis frequencies are lower at high AOD
549 levels (AOD > 1) than those at low AOD level (AOD < 1). This result means that the
550 negative feedback mechanism is prevalent throughout the whole campaign period.
551 Therefore, the prevention and control measures of air pollution in Beijing need to
552 incorporate this coupling mechanism between particulate matter and ozone to achieve
553 effective control of these two main pollutants.

554 **4. Conclusion**

555 Photolysis reactions are important driving forces for tropospheric photochemical
556 oxidation processes and ozone production. In this study, we explored in detail the
557 effects of aerosols on photolysis frequencies and ozone production in Beijing, based
558 on a long observation period of 4 years. We have found that:

559 (1) There is a strong correlation between PM_{2.5} and AOD, and the slope in
560 summer is smaller significantly than in winter, which indicates that aerosols
561 in summer have a more efficient extinction capacity than in winter.

562 (2) As AOD increased, the extinction effect of aerosol on photolysis frequencies
563 was decreased; this result was related to a higher proportion of scattering
564 aerosols under high AOD conditions than under low AOD conditions. The
565 slope of the correlation between photolysis frequencies and AOD indicates
566 that the aerosols in urban Beijing have a stronger extinction on actinic flux
567 than absorptive dust aerosols in the Mediterranean.

568 (3) The influence of AOD on photolysis frequencies was evaluated quantitatively
569 by establishing parametric equations. According to the parametric equation,
570 aerosols lead to a decrease in $j(\text{NO}_2)$ by 24.2% and 30.4% for summer and
571 winter, respectively, and the corresponding decrease in $j(\text{O}^1\text{D})$ by 27.3% and
572 32.6% respectively, compared to an aerosol-free atmosphere.

573 (4) In order to evaluate the effects of aerosols on ozone production rate, we
574 carried out an observation campaign in August 2012. The results show that
575 aerosols reduced the net ozone production rate by 25% by reducing the
576 photolysis frequencies. High concentrations of ozone gaseous precursors
577 were often accompanied by high concentrations of particulate matter, which,
578 to a large extent, inhibited excessive levels of ozone generation and reflected
579 the negative feedback effect of the atmospheric system. Therefore, the
580 influence of aerosol on photolysis frequencies and thus on the rate of
581 oxidation of VOCs and NOx to ozone and secondary aerosol is important for
582 determining the atmospheric effects of controlling the precursor emissions of
583 these two important air pollutants (aerosols and ozone).

584

585 **Author contribution**

586

Author	Contribution
Wenjie Wang	acquisition of data; analysis and interpretation of data; drafting the article and revising it critically
Min Shao	substantial contributions to conception and design; revising the article critically
Min Hu	collection of data
Limin Zeng	collection of data
Yusheng Wu	collection of data

587

588

589

590 **ACKNOWLEDGEMENTS**

591 This work was supported by the Major Program of the National Natural Science
592 Foundation of China [Grant number 91644222]. We thank Hongbin Chen and Philippe
593 Goloub for data management of AOD and other aerosol optical properties on
594 AERONET.

595

596 **Reference**

597 Barnarda, J. C., Chapman E G., Fasta, J. D., Schmelzera, J. R., Slusserb, J. R.,
598 Shetterc, R. E.: An evaluation of the FAST-Jphotolysis algorithm for predicting
599 nitrogen dioxide photolysis rates under clear and cloudy sky conditions,
600 ATMOSPHERIC ENVIRONMENT, 38, 3393-3403,

- 601 10.1016/j.atmosenv.2004.03.034, 2004.
- 602 Bais, A. F., Kazantzidis, A., Kazadzis, S., Balis, D. S., Zerefos, C. S., Meleti, C.
- 603 Deriving an effective aerosol single scattering albedo from spectral surface UV
- 604 irradiance measurements, ATMOSPHERIC ENVIRONMENT, 39, 1093-1102,
- 605 DOI: 10.1016/j.atmosenv.2004.09.080, 2005.
- 606 Bohn, B., Corlett, G. K., Gillmann, M., Sanghavi, S., Stange, G., Tensing, E.,
- 607 Vrekoussis, M., Bloss, W. J., Clapp, L. J., Kortner, M., Dorn, H. P., Monks, P. S.,
- 608 Platt, U., Plass-Dulmer, C., Mihalopoulos, N., Heard, D. E., Clemitshaw, K. C .,
- 609 Meixner, F. X., Prevot, A. S. H., Schmitt, R.: Photolysis frequency measurement
- 610 techniques: Results of a comparison within the ACCENT project,
- 611 ATMOSPHERIC CHEMISTRY AND PHYSICS, 8, 5373–5391,
- 612 doi:10.5194/acp-8-5373-2008, 2008.
- 613 Casasanta, G., di Sarra, A., Meloni, D., Monteleone, F., Pace, G., Piacentino, S.,
- 614 Sferlazzo, D.: Large aerosol effects on ozone photolysis in the Mediterranean,
- 615 ATMOSPHERIC ENVIRONMENT, 45, 3937-3943,
- 616 10.1016/j.atmosenv.2011.04.065, 2011.
- 617 Castro, T., Madronich, S., Rivale, S., Muhlia, A., Mar, B.: The influence of aerosols
- 618 on photochemical smog in Mexico City, ATMOSPHERIC ENVIRONMENT, 35,
- 619 1765-1772, 10.1016/S1352-2310(00)00449-0, 2001.
- 620 Chang, D, Song, Y, Liu, B.: Visibility trends in six megacities in China 1973–2007,
- 621 ATMOSPHERIC RESEARCH, 94, 161-167, 10.1016/j.atmosres.2009.05.006,
- 622 2009.
- 623 Che, H., Zhang, X., Li, Y., Zhou, Z., Qu, J. J., Hao, X.: Haze trends over the capital
- 624 cities of 31 provinces in China, 1981–2005, THEORETICAL AND APPLIED
- 625 CLIMATOLOGY, 97, 235-242, 10.1007/s00704-008-0059-8, 2009.
- 626 de Miranda, R., Andrade, M. F., Fattori, A. P.: Preliminary studies of the effect of
- 627 aerosols on nitrogen dioxide photolysis rates in the city of Sao Paulo, Brazil.
- 628 ATMOSPHERIC RESEARCH, 75, 135–148, 10.1016/j.atmosres.2004.12.004,
- 629 2005.

- 630 Dickerson, R. R., Kondragunta, S., Stenchikov, G., Civerolo, K. L., Doddridge, B. G.,
631 Holben, N.: The impact of aerosols on solar ultraviolet radiation and
632 photochemical smog, *Science*, 278, 827–830, 10.1126/science.278.5339.827,
633 1997.
- 634 Ehhalt, D. H., Rohrer, F.: Dependence of the OH concentration on solar UV,
635 *JOURNAL OF GEOPHYSICAL RESEARCH-ATMOSPHERES*, 105,
636 3565–3571, 10.1029/1999JD901070, 2000.
- 637 Finlayson-Pitts, B. J., Pitts, J. N.: *Chemistry of the Upper and Lower Atmosphere*.
638 Academic Press, New York, 2000.
- 639 Flynn, J., Lefer, B., Rappenglück, B., Leuchner, M., Perna, R., Dibb, J., Ziembka, L.,
640 Anderson, C., Stutz, J., Brune, W., Ren, X. R.: Impact of clouds and aerosols on
641 ozone production in Southeast Texas. *ATMOSPHERIC ENVIRONMENT*, 44,
642 4126–4133, 10.1016/j.atmosenv.2009.09.005, 2010.
- 643 Fotiadi, A., Hatzianastassiou, N., Drakakis, E., Matsoukas, C., Pavlakis, K. G.,
644 Hatzidimitriou, D., Gerasopoulos, E., Mihalopoulos, N., Vardavas, I.: Aerosol
645 physical and optical properties in the eastern Mediterranean Basin, Crete, from
646 Aerosol Robotic Network data, *ATMOSPHERIC CHEMISTRY AND PHYSICS*,
647 6, 5399–5413, 10.5194/acp-6-5399-2006, 2006
- 648 Gao W, Tie X X, Xu J M, Huang R J, Mao X Q, Zhou G Q, Luyu Chang. Long-term
649 trend of O₃ in a mega City (Shanghai), China: Characteristics, causes, and
650 interactions with precursors. *SCIENCE OF THE TOTAL ENVIRONMENT*, 603,
651 425–433, 10.1016/j.scitotenv.2017.06.099, 2017.
- 652 Garland, R.; O. Schmid, A.; Nowak, P.; Achtert, A.; Wiedensohler, S.; Gunthe, N.;
653 Takegawa, K.; Kita, Y.; Kondo, and M. Hu (2009), Aerosol optical properties
654 observed during Campaign of Air Quality Research in Beijing 2006
655 (CAREBeijing-2006): Characteristic differences between the inflow and outflow
656 of Beijing city air, *JOURNAL OF GEOPHYSICAL
657 RESEARCH-ATMOSPHERES*, 114, D00G04, 10.1029/2008JD010780, 2009.

- 658 Gerasopoulos, E., Kazadzis, S., Vrekoussis, M., Kouvarakis, G., Liakakou, E.,
659 Kouremeti, N., Giannadaki, D., Kanakidou, M., Bohn, B., Mihalopoulos, N.:
660 Factors affecting O₃ and NO₂ photolysis frequencies measured in the eastern
661 Mediterranean during the five-year period 2002–2006, JOURNAL OF
662 GEOPHYSICAL RESEARCH-ATMOSPHERES, 117, D22305,
663 10.1029/2012JD017622, 2012.
- 664 Goliff, W. S., Stockwell, W. R., Lawson, C. V.: The regional atmospheric chemistry
665 mechanism, version 2, ATMOSPHERIC ENVIRONMENT, 68: 174–185,
666 10.1016/j.atmosenv.2012.11.038, 2013.
- 667 Guo, S., Hu M, Zamora, M. L., Peng, J. F., Shang, D. J., Zheng, J., Du, Z. F., Wu, Z.
668 J., Shao, M., Zeng, L. M., Molina, M. J., Zhang, R. Y.: Elucidating severe urban
669 haze formation in China, PROCEEDINGS OF THE NATIONAL ACADEMY
670 OF SCIENCES OF THE UNITED STATES OF AMERICA, 111: 17373–17378,
671 10.1073/pnas.1419604111, 2014.
- 672 Han, T. T., Liu, X. G., Zhang, Y. H., Qu, Y., Gu, J. W., Ma, Q., Lu, K. D., Tian, H. Z.,
673 Chen, J., Zeng, L. M.: Characteristics of aerosol optical properties and their
674 chemical apportionments during CAREBeijing 2006, AEROSOL AND AIR
675 QUALITY RESEARCH, 14: 1431-1442, 10.4209/aaqr.2013.06.0203, 2014.
- 676 Han, T. T., Xu, W. Q., Chen, C., Liu, X. G., Wang, Q. Q., Li, J., Zhao, X. J., Du, W.,
677 Wang, Z. F., Sun, Y. L.: Chemical apportionment of aerosol optical properties
678 during the Asia-Pacific Economic Cooperation summit in Beijing, China,
679 JOURNAL OF GEOPHYSICAL RESEARCH-ATMOSPHERES, 120,
680 10.1002/2015JD023918, 2015b.
- 681 Han, T. T., Xu, W. Q., Li, J., Freedman, A., Zhao, J., Wang, Q. Q., Chen, C., Zhang, Y.
682 J., Wang, Z. F., Fu, P. Q.: Aerosol optical properties measurements by a CAPS
683 single scattering albedo monitor: Comparisons between summer and winter in
684 Beijing, China, JOURNAL OF GEOPHYSICAL RESEARCH-ATMOSPHERES,
685 122, 2513-2526, 10.1002/2016JD025762, 2017.
- 686 Han, T., Liu, X., Zhang, Y., Qu, Y., Zeng, L., Hu, M., Zhu, T.: Role of secondary

- 687 aerosols in haze formation in summer in the Megacity Beijing, JOURNAL OF
688 ENVIRONMENTAL SCIENCES, 31, 51-60, 10.1016/j.jes.2014.08.026, 2015a.
- 689 He, S., Carmichael, G. R.: Sensitivity of photolysis rates and ozone production in the
690 troposphere to aerosol properties, JOURNAL OF GEOPHYSICAL
691 RESEARCH-ATMOSPHERES, 104, 26307–26324, 10.1029/1999JD900789,
692 1999.
- 693 Hendrick, F; Muller, JF; Clemer, K; Wang, P; De Maziere, M; Fayt, C; Gielen, C;
694 Hermans, C; Ma, JZ; Pinardi, G ; Stavrakou, T; Vlemmix, T; Van Roozendael, M.,
695 Four years of ground-based MAX-DOAS observations of HONO and NO₂ in the
696 Beijing area. ATMOSPHERIC CHEMISTRY AND PHYSICS, 14(2), 765-781,
697 2014.
- 698 Hodzic, A., Madronich, S., Bohn, B., Massie, S., Menut, L., and Wiedinmyer, C.:
699 Wildfire particulate matter in Europe during summer 2003: meso-scale modeling
700 of smoke emissions, trans-port and radiative effects, ATMOSPHERIC
701 CHEMISTRY AND PHYSICS, 7, 4043–4064, 10.5194/acp-7-4043-2007, 2007.
- 702 Hofzumahaus, A., Kraus, A., Muller, M.: Solar actinic flux spectroradiometry: A
703 technique for measuring photolysis frequencies in the atmosphere, APPLIED
704 OPTICS, 38, 4443–4460, 10.1364/AO.38.004443, 1999.
- 705 Hofzumahaus, A., Lefer, B. L., Monks, P. S., Hall, S. R., Kylling, A., Mayer, B.,
706 Shetter, R. E., Junkermann, W., Bais, A., Calvert, J. G., Cantrell, C. A.,
707 Madronich, S., Edwards, G. D., Kraus, A.: Photolysis frequency of O₃ to O(¹D):
708 Measurements and modeling during the International Photolysis Frequency
709 Measurement and Modeling Intercomparison (IPMMI), JOURNAL OF
710 GEOPHYSICAL RESEARCH-ATMOSPHERES, 109 (D8), D08S90,
711 10.1029/2003JD004333, 2004.
- 712 Jacobson, M, Z.: Studying the effects of aerosols on vertical photolysis rate
713 coefficient and temperature profiles over an urban airshed, JOURNAL OF
714 GEOPHYSICAL RESEARCH-ATMOSPHERES, 103, 10593–10604,
715 10.1029/98JD00287, 1998.

- 716 Lefer, B. L., Shetter, R. E., Hall, S. R.: Impact of clouds and aerosols on photolysis
717 frequencies and photochemistry during TRACE-P: 1. Analysis using radiative
718 transfer and photochemical box models, JOURNAL OF GEOPHYSICAL
719 RESEARCH-ATMOSPHERES, 108, 8821-8835, 10.1029/2002JD003171, 2003.
- 720 Kazadzis, S., Bais, A. F., Balis, D., Zerefos, C. S., and Blumthaler, M. Retrieval of
721 down-welling UV actinic flux density spectra from spectral measurements of
722 global and direct solar UV irradiance, J. Geophys. Res., 105, 4857-4864, 2000.
- 723 Kazadzis, S., Topaloglou, C., Bais, A. F., Blumthaler, M., Balis, D., Kazantzidis, A.,
724 Schallhart, B. Actinic flux and O¹D photolysis frequencies retrieved from
725 spectral measurements of irradiance at Thessaloniki, Greece, ATMOSPHERIC
726 CHEMISTRY AND PHYSICS, 4, 2215-2226, DOI: 10.5194/acp-4-2215-2004,
727 2004.
- 728 Kazadzis, S., Amiridis, V., and Kouremeti, N. The Effect of Aerosol Absorption in
729 Solar UV Radiation, Advances in Meteorology, Climatology and Atmospheric
730 Physics, 1041-1047, 2012.
- 731 Krotkov, N., Bhartia, P. K., Herman, J., Slusser, J., Scott, G., Labow, G., Vasilkov, A.
732 P., Eck, T. F., Dubovik, O., Holben, B. N. Aerosol ultraviolet absorption
733 experiment (2000 to 2004), part 2: Absorption optical thickness, refractive index,
734 and single scattering albedo, OPTICAL ENGINEERING, 44, 4, 041005. DOI:
735 10.1117/1.1886819, 2005.
- 736 Kylling, A., Webb, A. R., Bais, A. F., Blumthaler, M., Schmitt, R., Thiel, S.,
737 Kazantzidis, A., Kift, R., Misslebeck, M., Schallhart, B., Schreder, J., Topaloglou,
738 C., Kazadzis, S., and Rimmer, J.: Actinic flux determination from measurements
739 of irradiance, J. Geophys. Res., 108 (D16), 4506-4515, 2003.
- 740 Li C C, Mao J T, Liu Q H. Using MODIS to study the distribution and seasonal
741 variation of aerosol optical thickness in eastern China. Science Bulletin (China),
742 48: 2094-2100. 2003.
- 743 Li, J., Wang, Z. F., Wang, X., Yamaji, K., Takigawa, M., Kanaya, Y., Pochanart, P.,
744 Liu, Y., Irie, H., Hu, B., Tanimoto, H., Akimoto, H.: Impacts of aerosols on

- 745 summertime tropospheric photolysis frequencies and photochemistry over
746 Central Eastern China, ATMOSPHERIC ENVIRONMENT, 45: 1817-1829,
747 10.1016/j.atmosenv.2011.01.016, 2011.
- 748 Liao, H., Yung, Y. L., and Seinfeld, J. H.: Effects of aerosols on tropospheric
749 photolysis rates in clear and cloudy atmospheres, JOURNAL OF
750 GEOPHYSICAL RESEARCH, 104(D19), 23697–23707, 1999.
- 751 Liu, Q.Y., Ma, T. M., Olson, M. R., Liu, Y. J., Zhang, T. T., Wu, Y., Schauer, J. J.:
752 Temporal variations of black carbon during haze and non-haze days in Beijing,
753 SCIENTIFIC REPORTS, 6, 33331, 10.1038/srep33331, 2016.
- 754 Lou, S. J; Liao, H; Zhu, B. Impacts of aerosols on surface-layer ozone concentrations
755 in China through heterogeneous reactions and changes in photolysis rates.
756 ATMOSPHERIC ENVIRONMENT, 85:123-138,
757 0.1016/j.atmosenv.2013.12.004, 2014.
- 758 Lu, K. D., Rohrer, F., Holland, F., Fuchs, H., Bohn, B., Brauers, T., Chang, C. C.,
759 Häseler, R., Hu, M., Kita, K., Kondo, Y., Li, X., Lou, S. R., Nehr, S., Shao, M.,
760 Zeng, L. M., Wahner, A., Zhang, Y. H., Hofzumahaus, A.: Observation and
761 modelling of OH and HO₂ concentrations in the Pearl River Delta 2006: a
762 missing OH source in a VOC rich atmosphere, ATMOSPHERIC CHEMISTRY
763 AND PHYSICS, 12: 1541-1569, 10.5194/acp-12-1541-2012, 2012
- 764 Ma, X. Y., Wang, J. Y., Yu, F. Q., Jia, H. L., Hu, Y. N.: Can MODIS AOD be
765 employed to derive PM_{2.5} in Beijing-Tianjin-Hebei over China?
766 ATMOSPHERIC RESEARCH, 181, 250-256, 10.1016/j.atmosres.2016.06.018,
767 2016.
- 768 Ma, Z. W., Hu, X. F., Huang, L., Bi, J., Liu, Y.: Estimating Ground-Level PM_{2.5} in
769 China Using Satellite Remote Sensing. Environ Sci Technol, 48: 7436–7444.
- 770 Madronich, S, The Atmosphere and UV-B Radiation at Ground Level, Environmental
771 UV Photobiology, doi: 0.1007/978-1-4899-2406-3_1. 1993,

- 772 Madronich, S., and S. Flocke, The role of solar radiation in atmospheric chemistry, in
773 Environmental Photochemistry, edited by P. Boule, pp. 1-26, Springer-Verlag,
774 New York, 1999.
- 775 Mailler, S., Menut, L., di Sarra, A. G., Becagli, S., Di Iorio, T., Bessagnet, B., Briant,
776 R., Formenti, P., Doussin, J. F., Gomez-Amo, J. L., Mallet, M., Rea, G., Siour,
777 G., Sferlazzo, D. M., Traversi, R., Udisti, R., Turquety, S.: On the radiative
778 impact of aerosols on photolysis rates: comparison of simulations and
779 observations in the Lampedusa island during the ChArMEx/ADRIMED
780 campaign, ATMOSPHERIC CHEMISTRY AND PHYSICS, 16(3):1219-1244,
781 10.5194/acp-16-1219-2016, 10.5194/acp-16-1219-2016, 2016.
- 782 Peeters, J., Nguyen, T. L., Vereecken, L.: HOX radical regeneration in the oxidation
783 of isoprene. PHYSICAL CHEMISTRY CHEMICAL PHYSICS, 11: 5935-5939,
784 10.1039/b908511d, 2009.
- 785 Pere, J. C., Bessagnet, B., Pont, V., Mallet, M., Minvielle, F.: Influence of the aerosol
786 solar extinction on photochemistry during the 2010 Russian wildfires episode,
787 ATMOSPHERIC CHEMISTRY AND PHYSICS, 15, 10983-10998,
788 10.5194/acp-15-10983-2015, 2015.
- 789 Raga, G. B., Castro, T., Baumgardner, D.: The impact of megacity pollution on local
790 climate and implications for the regional environment: Mexico City,
791 ATMOSPHERIC ENVIRONMENT, 35, 1805-1811,
792 10.1016/S1352-2310(00)00275-2, 2001.
- 793 Real, E. and Sartelet, K.: Modeling of photolysis rates over Europe: impact on
794 chemical gaseous species and aerosols, ATMOSPHERIC CHEMISTRY AND
795 PHYSICS, 11, 1711–1727, 10.5194/acp-11-1711-2011, 2011.
- 796 Rohrer, F; Lu, K. D; Hofzumahaus, A; Bohn, B ; Brauers, T ; Chang, C. C ; Fuchs, H;
797 Haseler, R; Holland, F; Hu, M., Maximum efficiency in the
798 hydroxyl-radical-based self-cleansing of the troposphere, Nature Geoscience. 7,
799 559-563, 2014.

800 Shetter, R. E., Muller, M.: Photolysis frequency measurements using actinic flux
801 spectroradiometry during PEM-Tropics Mission: Instrumentation description and
802 some results, JOURNAL OF GEOPHYSICAL RESEARCH-ATMOSPHERES,
803 104, 5647-5661, 10.1029/98JD01381, 1999.

804 Shetter, R. E.: Photolysis frequency of NO₂: measurement and modeling during the
805 International Photolysis Frequency Measurement and Modeling Intercomparison
806 (IPMMI), JOURNAL OF GEOPHYSICAL RESEARCH-ATMOSPHERES, 108,
807 8544, 10.1029/2002JD002932, 2003.

808 Stone, D; Whalley, L. K; Heard, D. E. Tropospheric OH and HO₂ radicals: field
809 measurements and model comparisons, Chem. Soc. Rev.,41(19): 6348-6404,
810 10.1039/c2cs35140d, 2012.

811 Tang, Y., Carmichael, G. R., Kurata, G., Uno, I., Weber, R. J., Song, C. H., Guttikunda,
812 S. K., Woo, J. H., Streets, D. G., Wei, C., Clarke, A. D., Huebert, B., Anderson, T.
813 L.: Impacts of dust on regional tropospheric chemistry during the ACE-Asia
814 experiment: a model study with observations, JOURNAL OF GEOPHYSICAL
815 RESEARCH-ATMOSPHERES, 109, D19S21, 10.1029/2003JD003806, 2004.

816 Tian, P., Wang, G. F., Zhang, R. J., Wu, Y. F., Yan, P.: Impacts of aerosol chemical
817 compositions on optical properties in urban Beijing, China, PARTICUOLOGY,
818 18, 155-164, 10.1016/j.partic.2014.03.014, 2015.

819 Tie, X. X., Madronich, S., Walters, S., Edwards, D. P., Ginoux, P., Mahowald, N.,
820 Zhang, R. Y., Lou, C., Brasseur, G.: Assessment of the global impact of aerosols
821 on tropospheric oxidants. JOURNAL OF GEOPHYSICAL
822 RESEARCH-ATMOSPHERES, 110, D03204, 10.1029/2004JD005359, 2005.

823 Topaloglou, C., Kazadzis, S., Bais, AF., Blumthaler, M., Schallhart, B., Balis, D. NO₂
824 and HCHO photolysis frequencies from irradiance measurements in Thessaloniki,
825 Greece. ATMOSPHERIC CHEMISTRY AND PHYSICS, 5, 1645-1653, DOI:
826 10.5194/acp-5-1645-2005, 2005. Trebs, I., Bohn, B., Ammann, C., Rummel, U.,
827 Blumthaler, M., Konigstedt, R., Meixner, F. X., Fan, S., Andreae, M. O.
828 Relationship between the NO₂ photolysis frequency and the solar global

- 829 irradiance, ATMOSPHERIC MEASUREMENT TECHNIQUES, 2, 725-739,
830 DOI: 10.5194/amt-2-725-2009, 2009.
- 831 van Donkelaar, A., Martin, R. V., Brauer, M., Kahn, R., Levy, R., Verduzco, C., and
832 Villeneuve, P. J.: Global Estimates of Ambient Fine Particulate Matter
833 Concentrations from Satellite-Based Aerosol Optical Depth: Development and
834 Application. Environmental Health Perspectives, 118, 847-855,
835 10.1289/ehp.0901623, 2010.
- 836 Verstraeten, W, W., Neu, J. L., Williams, J. E., Bowman, K. W., Worden, J. R.,
837 Boersma, K. F.: Rapid increases in tropospheric ozone production and export
838 from China. NATURE GEOSCIENCE, 8, 690-695, 10.1038/NGEO2493, 2015.
- 839 Volkamer R, Sheehy P, Molina L T, Molina M J.: Oxidative capacity of the Mexico
840 City atmosphere – Part 1: A radical source perspective, ATMOSPHERIC
841 CHEMISTRY AND PHYSICS, 10, 6969–6991, 10.5194/acp-10-6969-2010,
842 2010.
- 843 Wang, B., Shao, M., Lu, S. H., Yuan, B., Zhao, Y., Wang, M., Zhang, S. Q., Wu, D.:
844 Variation of ambient non-methane hydrocarbons in Beijing city in summer 2008,
845 ATMOSPHERIC CHEMISTRY AND PHYSICS, 10, 5911–5923,
846 10.5194/acp-10-5911-2010, 2010.
- 847 Wang, Q., Sun, Y., Jiang, Q., Du, W., Sun, C., Fu, P., Wang, Z.: Chemical
848 composition of aerosol particles and light extinction apportionment before and
849 during the heating season in Beijing, China. JOURNAL OF GEOPHYSICAL
850 RESEARCH-ATMOSPHERES, 120: 12,708-12,722, 10.1002/2015JD023871,
851 2015.
- 852 Xin, J. Y; Gong, C. S; Liu, Z. R; Cong, Z. Y; Gao, W. K; Song, T; Pan, Y. P; Sun, Y;
853 Ji, D. S; Wang, L. L; Tang, G. Q; Wang, Y. S.: The observation-based
854 relationships between PM_{2.5} and AOD over China, JOURNAL OF
855 GEOPHYSICAL RESEARCH-ATMOSPHERES, 121, 10701-10716,
856 10.1002/2015JD024655, 2016.

- 857 Xu, J., Ma, J. Z., Zhang, X. L., Xu, X. B., Xu, X. F., Lin, W. L., Wang, Y., Meng, W.,
858 and Ma, Z. Q.: Measurements of ozone and its precursors in Beijing during
859 summertime: impact of urban plumes on ozone pollution in downwind rural
860 areas, ATMOSPHERIC CHEMISTRY AND PHYSICS, 11, 12241–12252,
861 10.5194/acp-11-12241-2011, 2011.
- 862 Zhang, J. P., Zhu, T., Zhang, Q. H., Li, C. C., Shu, H. L., Ying, Y., Dai, Z. P., Wang, X.,
863 Liu, X. Y., Liang, A. M., Shen, H. X., and Yi, B. Q.: The impact of circulation
864 patterns on regional transport pathways and air quality over Beijing and its
865 surroundings, ATMOSPHERIC CHEMISTRY AND PHYSICS, 12, 5031–5053,
866 10.5194/acp-12-5031-2012, 2012.
- 867 Zhang, L.; Shao, J.; Lu, X.; Zhao, Y.; Hu, Y.; Henze, D. K.; Liao, H.; Gong, S.; Zhang,
868 Q.: Sources and Processes Affecting Fine Particulate Matter Pollution over North
869 China: An Adjoint Analysis of the Beijing APEC Period. ENVIRONMENTAL
870 SCIENCE & TECHNOLOGY, 50(16), 8731-8740, 10.1021/acs.est.6b03010,
871 2016.
- 872 Zhang, Q., Yuan, B., Shao, M., Wang, X., Lu, S., Lu, K., Wang, M., Chen, L., Chang,
873 C. C., Liu, S. C.: Variations of ground-level O₃ and its precursors in Beijing in
874 summertime between 2005 and 2011, ATMOSPHERIC CHEMISTRY AND
875 PHYSICS, 14, 6089-6101, 10.5194/acp-14-6089-2014, 2014.
- 876 Zhang, R., Jing, J., Tao, J., Hsu, S. C., Wang, G., Cao, J., Lee, C. S. L., Zhu, L., Chen,
877 Z., Zhao, Y., Shen, Z.: Chemical characterization and source apportionment of
878 PM_{2.5} in Beijing: seasonal perspective, ATMOSPHERIC CHEMISTRY AND
879 PHYSICS, 13, 7053-7074, 10.5194/acp-13-7053-2013, 2013.
- 880 Zheng, C. W., Zhao, C. F., Zhu, Y. N., Wang, Y., Shi, X. Q., Wu, X. L., Chen, T. M.,
881 Wu, F., Qiu, Y. M.: Analysis of influential factors for the relationship between
882 PM_{2.5} and AOD in Beijing, ATMOSPHERIC CHEMISTRY AND PHYSICS, 17,
883 13473-13489, 10.5194/acp-17-13473-2017, 2017.
- 884
- 885

886
887
888
889
890
891
892
893
894

895 Table 1. Instruments deployed in the field campaign undertaken in August 2012 and
896 used for data analysis.

Parameters	Measurement technique	Time resolution	Detection limit	Accuracy
j(O ¹ D) and j(NO ₂)	Spectroradiometer	10 s	/	± 10%
O ₃	UV photometry	60 s	0.5 ppbv	± 5%
NO	Chemiluminescence	60 s	60 pptv	± 20%
NO ₂	Chemiluminescence	60 s	300 pptv	± 20%
CO	IR photometry	60 s	4 ppb	± 5%
SO ₂	Pulsed UV fluorescence	60 s	0.1 ppbv	± 5%
HCHO	Hantzsch fluorimetry	60 s	25 pptv	± 5%
VOCs	GC-FID/MS	1 h	20-300 pptv	± 15~20%

897
898
899
900
901
902

903

904

905

906

907

908

909

910

911

912

913 Table 2. O₃ column concentration, temperature, relative humidity and respective
 914 standard deviation for different seasons.

915

	O ₃ column (Du)	Temperature (°C)	Relative humidity (%)
Spring	354.9±37.3	15.6±7.8	33.2±18.1
Summer	310.2±23.8	27.5±4.2	57.2±17.7
Autumn	303.8±22.8	15.5±7.4	46.4±20.6
Winter	347.2±28.2	0.53±4.24	30.4±17.6

916

917

918

919

920

921

922

923

924

925

926

927

928

929

930

931

932

933

934 Table 3. Slope, intercept and the square of correlation coefficient (r^2) of linear fits of
 935 correlation between $j(O^1D)$ and AOD for each ozone column class at AOD smaller
 936 than 0.7.

O_3 column (DU)	SZA=30°			SZA=60°		
	Slope ($10^{-6}s^{-1}$)	Intercept ($10^{-6}s^{-1}$)	r^2	Slope ($10^{-6}s^{-1}$)	Intercept ($10^{-6}s^{-1}$)	r^2
300-330	-6.24±1.52	25.7±0.8	0.34	-4.21±0.43	7.67±0.33	0.41
330-360	-6.50±1.43	23.2±0.6	0.40	-5.01±0.34	7.15±0.21	0.52
360-390	-9.45±1.64	20.9±0.9	0.52	-6.93±0.62	7.59±0.34	0.66

937

938

939

940

941

942

943

944

945

946

947

948

949

950

951 Table 4. Slope, intercept and the square of correlation coefficient (r^2) of linear fits of
 952 correlation between $j(\text{NO}_2)$ and AOD for each ozone column class at AOD smaller
 953 than 0.7.

$\cos(\text{SZA})$	Slope (10^{-3} s^{-1})	Intercept (10^{-3} s^{-1})	r^2
0-0.2	-1.28±0.07	1.54±0.04	0.52
0.2-0.4	-2.44±0.10	3.40±0.04	0.41
0.4-0.6	-3.20±0.09	5.49±0.04	0.49
0.6-0.8	-2.08±0.09	7.20±0.05	0.38
0.8-1.0	-1.77±0.12	8.12±0.05	0.26

954

955

956

957

958

959

960

961

962

963

964

965

966

967

968

969 Table 5. The fitting parameters a_1-a_6 and determination coefficients of E5 for $j(\text{NO}_2)$.

O_3 column (DU)	a_1	a_2	a_3	a_4	a_5	a_6	r^2
270-300	-0.20 ± 0.09	-2.1 ± 0.1	13.1 ± 0.4	0.27 ± 0.02	0.19 ± 0.09	-3.5 ± 0.3	0.96
300-330	-0.48 ± 0.07	-1.9 ± 0.1	13.3 ± 0.3	0.19 ± 0.01	0.34 ± 0.08	-3.9 ± 0.3	0.96
330-360	-0.22 ± 0.08	-2.2 ± 0.1	11.8 ± 0.3	0.42 ± 0.03	0.23 ± 0.03	-2.6 ± 0.2	0.96
360-400	-0.21 ± 0.10	-2.0 ± 0.1	12.6 ± 0.2	0.18 ± 0.02	0.39 ± 0.03	-4.0 ± 0.3	0.95

970

971 Table 6. The fitting parameters a_1-a_6 and determination coefficients of E5 for $j(\text{O}^1\text{D})$.

O_3 column (DU)	a_1	a_2	a_3	a_4	a_5	a_6	r^2
270-300	0.88 ± 0.30	-0.10 ± 0.21	-5.1 ± 0.5	0.93 ± 0.06	-8.6 ± 0.4	43.9 ± 0.8	0.96
300-330	0.58 ± 0.07	0.13 ± 0.17	-3.8 ± 0.8	0.68 ± 0.04	-7.1 ± 0.2	37.1 ± 0.8	0.96
330-360	2.2 ± 0.20	-0.65 ± 0.19	-9.8 ± 0.9	1.01 ± 0.07	-6.3 ± 0.3	38.1 ± 0.6	0.97
360-400	2.0 ± 0.10	-0.72 ± 0.40	-7.0 ± 0.5	0.76 ± 0.08	-6.2 ± 0.7	33.0 ± 0.8	0.95

972

973

974

975

976

977

978

979

980

981 Table 7. Mean and standard deviation of observed data during daytime (6:00–18:00)
 982 for A day and B day.

Observed data	A day: August 21, 2012	B day: August 26, 2012
AOD	0.21 ± 0.05	3.2 ± 0.4
PM _{2.5} ($\mu\text{g m}^{-3}$)	21.6 ± 9.0	125.0 ± 15.7
O ₃ column (Du)	302 ± 3.0	301 ± 3.0
Temperature($^{\circ}\text{C}$)	27.6 ± 3.3	27.6 ± 3.2
Relative humidity (%)	47.6 ± 10.1	54.5 ± 11.8
j(O ¹ D)(s^{-1})	$1.57 \times 10^{-5} \pm 1.24 \times 10^{-5}$	$6.87 \times 10^{-6} \pm 5.2 \times 10^{-6}$
j(NO ₂)(s^{-1})	$5.37 \times 10^{-3} \pm 2.88 \times 10^{-3}$	$2.87 \times 10^{-3} \pm 1.65 \times 10^{-3}$
O ₃ (ppb)	39.7 ± 16.56	86.8 ± 52.82
NO ₂ (ppb)	10.7 ± 5.0	24.9 ± 9.6
CO (ppm)	0.24 ± 0.05	0.85 ± 0.14
VOC reactivity (s^{-1})	3.0 ± 0.7	6.4 ± 1.7
HCHO (ppb)	2.7 ± 1.1	7.4 ± 1.9

983

984

985

986

987

988 Table 8. Monthly mean and standard deviation of observed data during daytime
 989 (6:00–18:00) under the condition of AOD less than 1 and larger than 1 in August 2012

Observed data	AOD<1	AOD>1
AOD	0.43 ± 0.24	2.0 ± 0.8
PM _{2.5} ($\mu\text{g m}^{-3}$)	26.4 ± 12.4	76.9 ± 47.1
O ₃ column (Du)	303 ± 4.0	302 ± 5.0
Temperature(°C)	29.6 ± 4.3	29.2 ± 4.1
Relative humidity (%)	42.1 ± 15.8	57.0 ± 12.8
j(O ¹ D)(s ⁻¹)	$1.62 \times 10^{-5} \pm 1.05 \times 10^{-5}$	$1.03 \times 10^{-5} \pm 0.67 \times 10^{-5}$
j(NO ₂)(s ⁻¹)	$5.64 \times 10^{-3} \pm 2.42 \times 10^{-3}$	$3.80 \times 10^{-3} \pm 1.66 \times 10^{-3}$
O ₃ (ppb)	52.4 ± 33.8	67.9 ± 45.7
NO ₂ (ppb)	16.4 ± 7.8	24.4 ± 8.9
CO (ppm)	0.47 ± 0.20	0.95 ± 0.47
VOC reactivity (s ⁻¹)	4.3 ± 1.7	6.2 ± 2.2
HCHO (ppb)	4.0 ± 1.4	6.5 ± 1.9

990

991

992

993

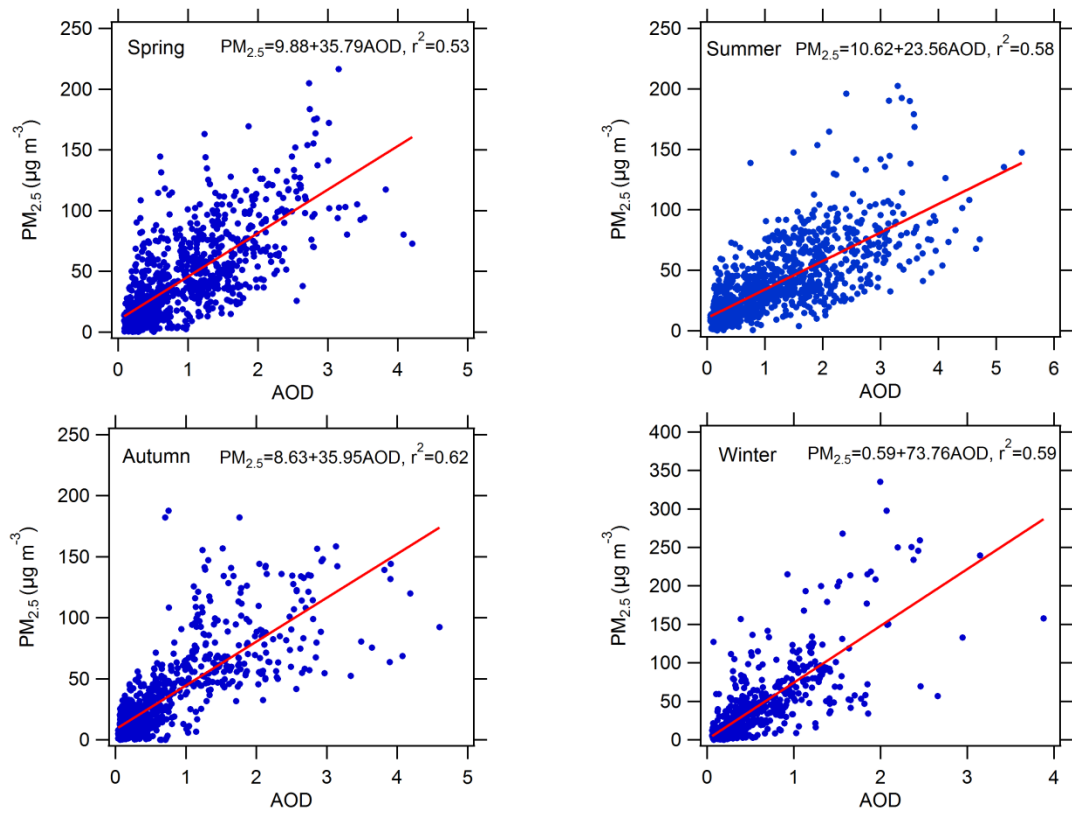
994

995

996

997

998



999

1000 Figure 1. Scatter plots between AOD at 380nm and $\text{PM}_{2.5}$ in four different seasons.
 1001 The slope, intercept and determination coefficient (r^2) were calculated.

1002

1003

1004

1005

1006

1007

1008

1009

1010

1011

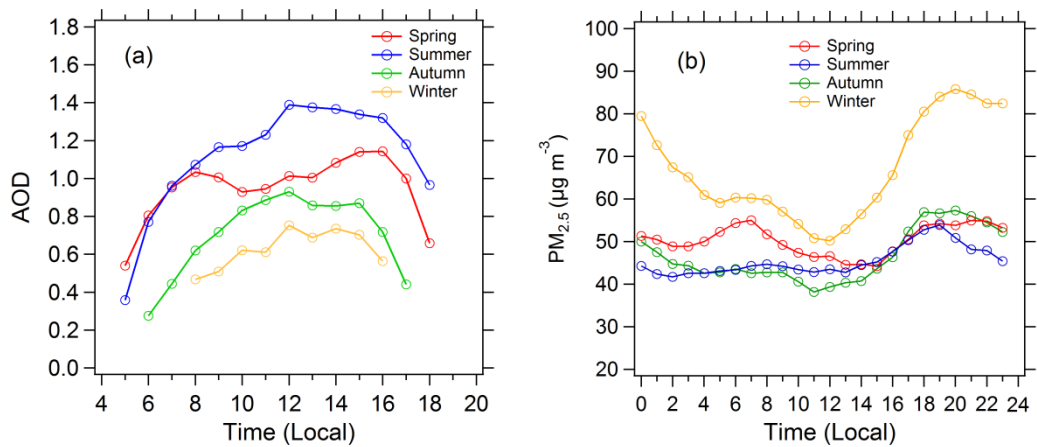
1012

1013

1014

1015

1016



1017

1018 Figure 2. Diurnal cycles of (a) mean AOD (380nm) and (b) mean $\text{PM}_{2.5}$ in four

1019 seasons.

1020

1021

1022

1023

1024

1025

1026

1027

1028

1029

1030

1031

1032

1033

1034

1035

1036

1037

1038

1039

1040

1041

1042 Figure 3. Diurnal cycles of (a) mean $j(O^1D)$ and (b) mean $j(NO_2)$ in four seasons

1043 under cloudless conditions.

1044

1045

1046

1047

1048

1049

1050

1051

1052

1053

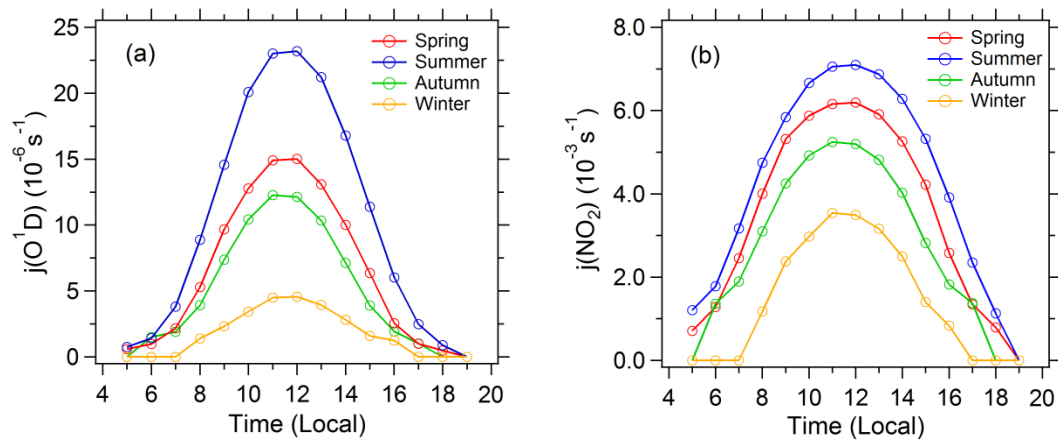
1054

1055

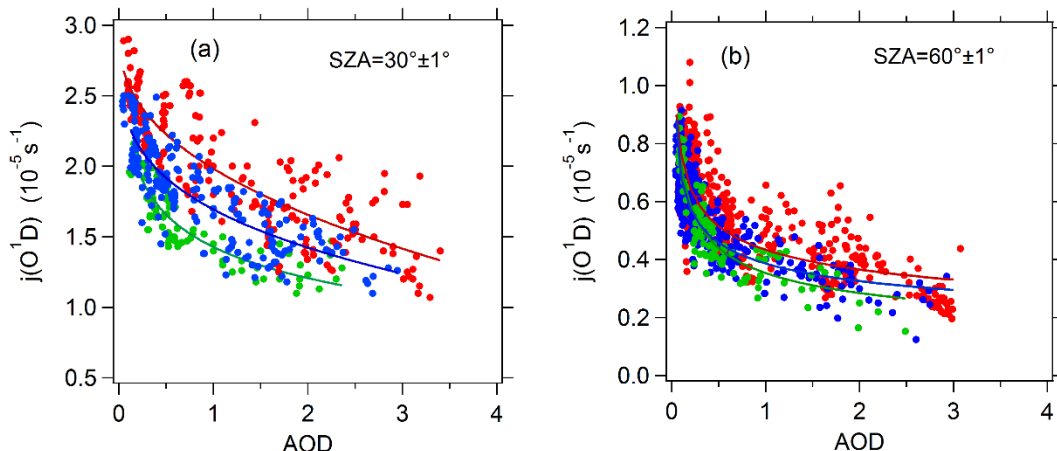
1056

1057

1058



1059
1060
1061
1062
1063
1064

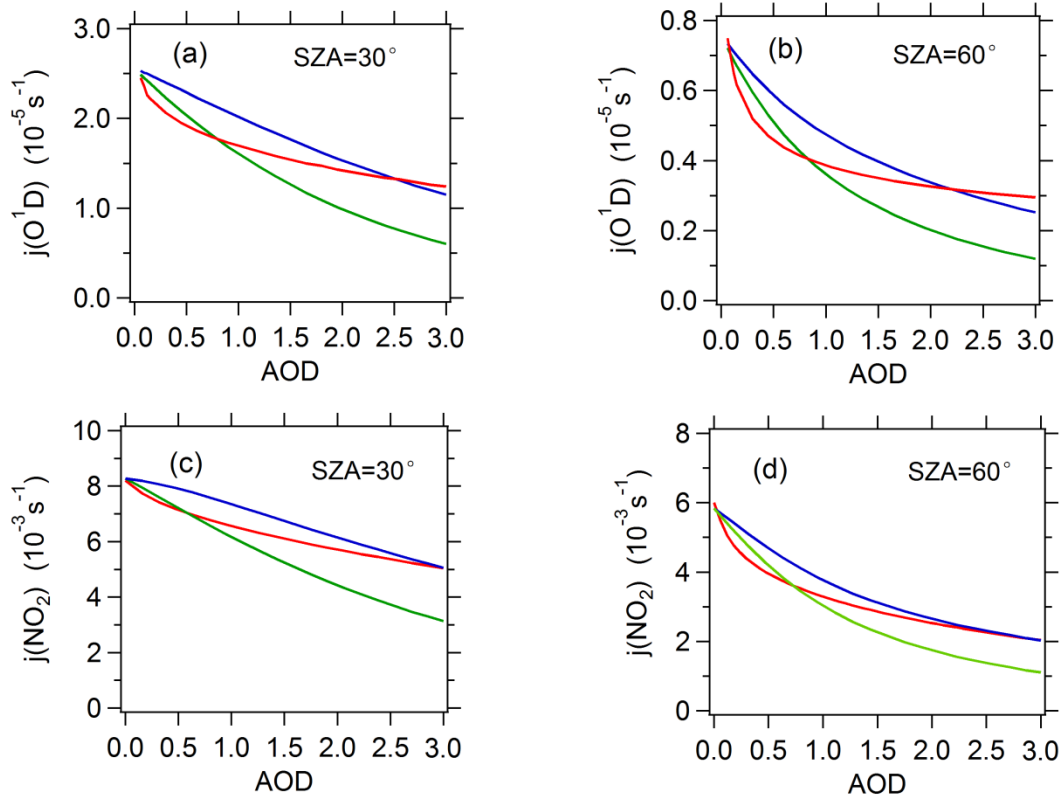


1065

1066 Figure 4. Dependence of $j(O^1D)$ on AOD at SZA of (a) 30° and (b) 60° and at
1067 different classes of ozone column concentration: 300-330 DU (red), 330-360 DU
1068 (blue), and 360-390 DU (green).

1069
1070
1071
1072
1073
1074
1075
1076
1077
1078
1079

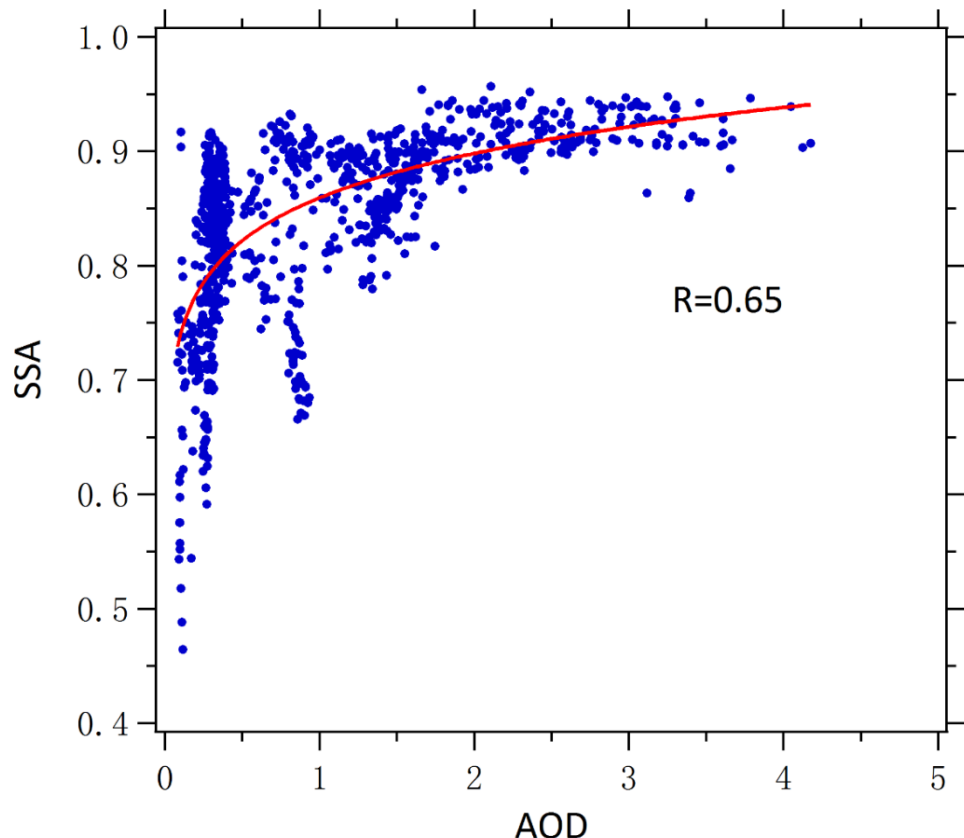
1080
1081
1082
1083
1084



1085
1086
1087
1088
1089
1090
1091
1092
1093
1094
1095

Figure 5. The relationship between observed or TUV-simulated photolysis frequencies and AOD at SZA of 30° and 60°. The red line represents observed average photolysis frequencies; the blue line and green line represents TUV-simulated photolysis frequencies at SSA of 0.95 and 0.85 respectively.

1096
1097
1098
1099
1100



1101

1102 Figure 6. Correlation between SSA and AOD observed in August 2012.

1103
1104
1105
1106
1107
1108
1109
1110
1111

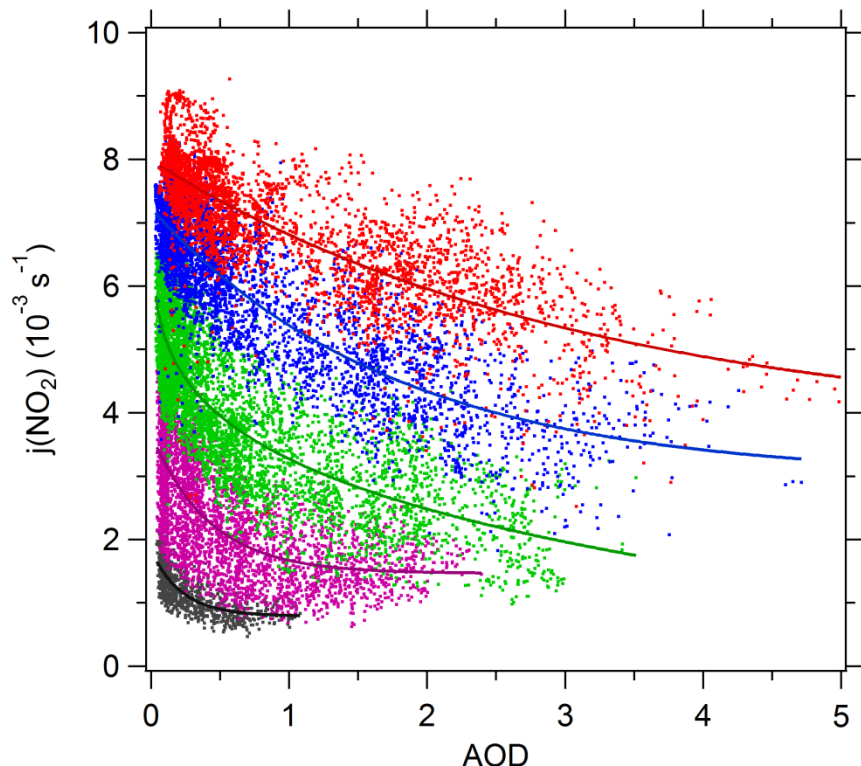
1112

1113

1114

1115

1116



1117

1118 Figure 7. Dependence of $j(\text{NO}_2)$ on AOD at different SZA classes. The classes of
1119 $\cos(\text{SZA})$ are $0 - 0.2$ (black), $0.2 - 0.4$ (purple), $0.4 - 0.6$ (green), $0.6 - 0.8$ (blue), and
1120 $0.8 - 1$ (red).

1121

1122

1123

1124

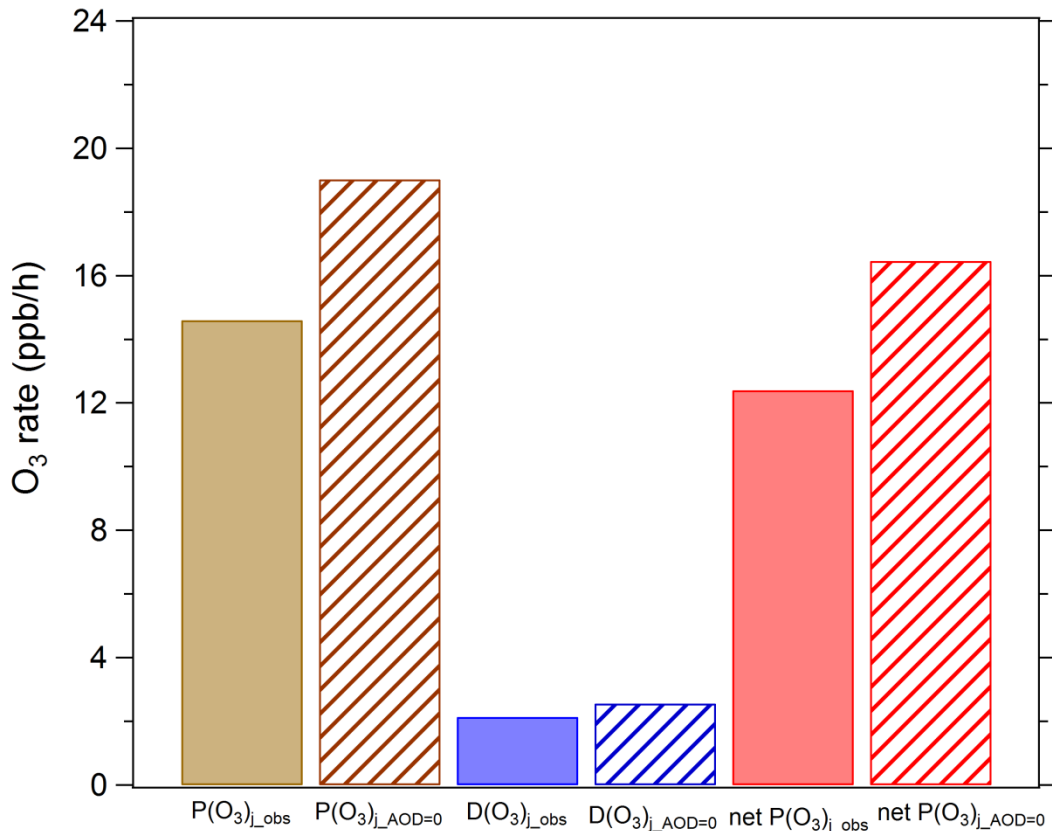
1125

1126

1127

1128

1129
1130
1131

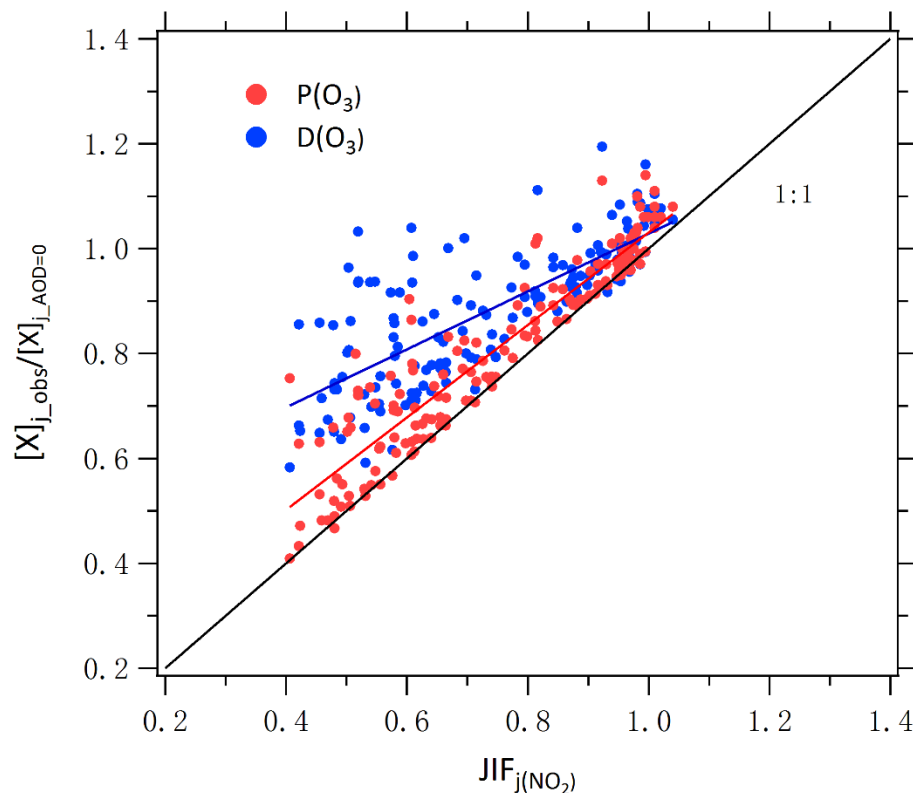


1132
1133 Figure 8. Average ozone production and loss terms in August 2012. P(O₃)_j_obs,
1134 D(O₃)_j_obs and net P(O₃)_j_obs represents ozone production rate, ozone loss rate, and net
1135 ozone production rate under observed photolysis frequencies; P(O₃)_j_AOD=0, D(O₃)
1136 j_AOD=0 and net P(O₃)_j_AOD=0 represents ozone production rate, ozone loss rate, and net
1137 ozone production rate under calculated photolysis frequencies when AOD is equal to
1138 0.

1139
1140
1141
1142

1143

1144



1145

1146 Figure 9. Correlation between $P(O_3)_{j_obs}/P(O_3)_{j_AOD=0}$ (or $D(O_3)_{j_obs}/D(O_3)_{j_AOD=0}$) and
1147 JIF of $j(\text{NO}_2)$.

1148

1149

1150

1151

1152

1153

1154

1155

1156

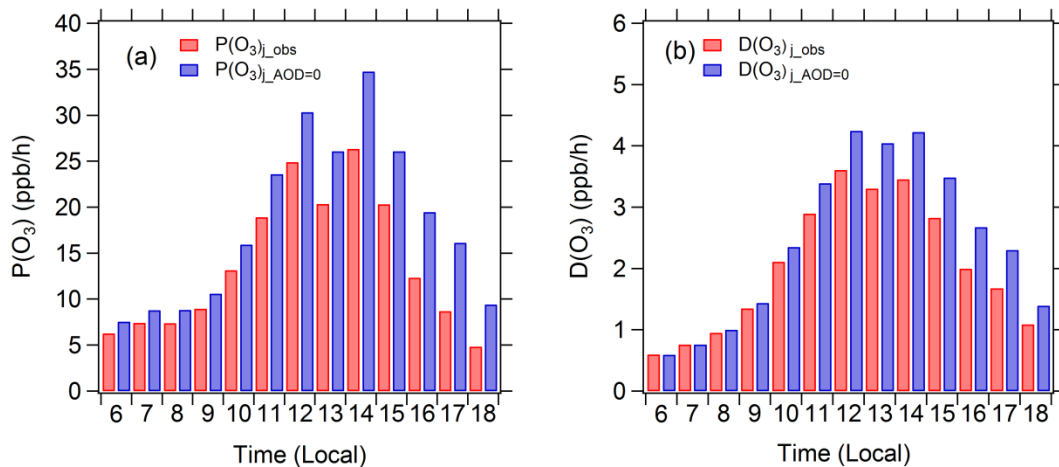
1157

1158

1159

1160

1161



1162

1163 Figure 10. Diurnal profiles of mean $P(O_3)_j_{obs}$, $P(O_3)_j_{AOD=0}$, $D(O_3)_j_{obs}$, and
1164 $D(O_3)_j_{AOD=0}$.

1165

1166

1167

1168

1169

1170

1171

1172

1173

1174

1175

1176

1177

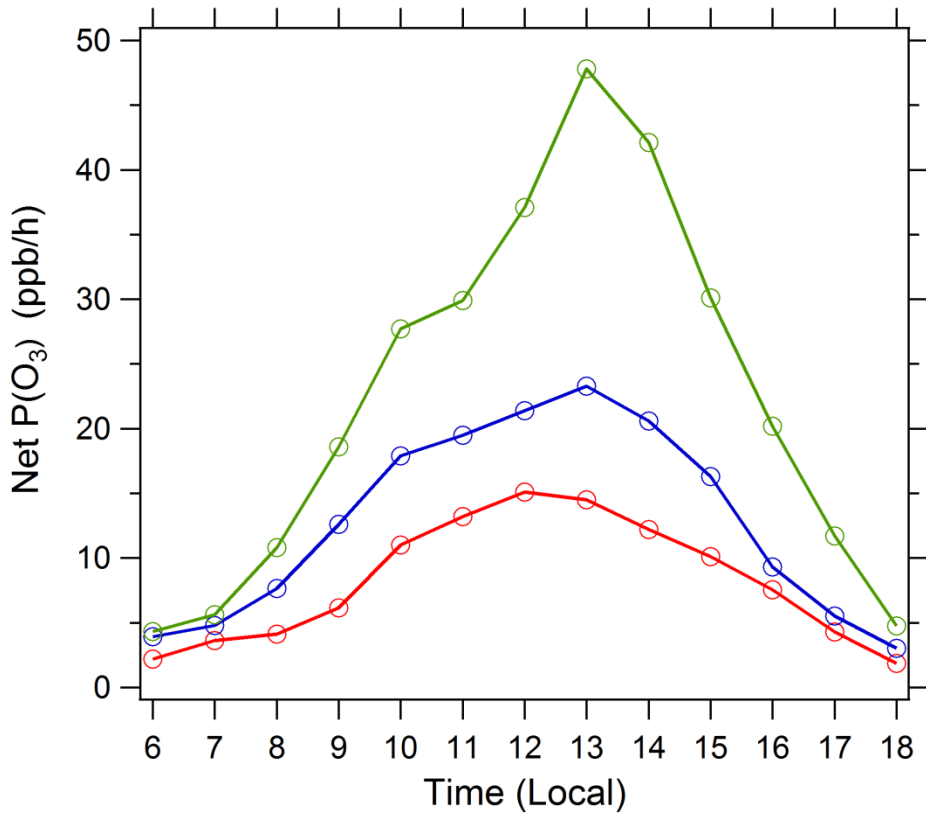
1178

1179

1180

1181

1182
1183
1184
1185



1186

1187 Figure 11. Diurnal profile of net $P(O_3)$ simulated by the box model. Three cases are
1188 displayed: (1) A day (red circles); (2) B day (blue circles); and (3) the photolysis
1189 frequencies of B day adjusted to the level of A day with other conditions unchanged
1190 (green circles).

1191